NASA CONTRACTOR REPORT

NASA CR-2431

NASA CR-2431

ACOUSTIC SOUNDING IN THE PLANETARY BOUNDARY LAYER

by Edward H. Kelly

Prepared by
UNIVERSITY OF OKLAHOMA
Norman, Okla. 73069
for George C. Marshall Space Flight Center

NATIONAL AERONAUTICS AND SPACE ADMINISTRATION • WASHINGTON, D. C. • MAY 1974

1. REPORT NO.	2. GOVERNMENT ACCESSION NO.	3. RECIPIENT'S CATALOG NO.
CR-2431		

4. TITLE AND SUBTITLE	5. REPORT DATE
Acoustic Sounding in the Planetary Boundary Layer	May 1974
	6. PERFORMING ORGANIZATION CODE M127
7. AUTHOR(S) Edward H. Kelly	8. PERFORMING ORGANIZATION REPORT #
9. PERFORMING ORGANIZATION NAME AND ADDRESS University of Oklahoma Norman, Oklahoma 73069	10. WORK UNIT NO.
	11. CONTRACT OR GRANT NO. NAS8-28659
12. SPONSORING AGENCY NAME AND ADDRESS National Aeronautics and Space Administration Washington, D.C. 20546	13. TYPE OF REPORT & PERIOD COVERED Contractor
	14. SPONSORING AGENCY CODE

15. SUPPLEMENTARY NOTES

Prepared under the technical monitorship of the Aerospace Environment Division, Aero-Astrodynamics Laboratory, NASA-Marshall Space Flight Center.

16. ABSTRACT

Three case studies are presented involving data from an acoustic radar. The first two cases examine data collected during the passage of a mesoscale cold-air intrusion, probably thunderstorm outflow, and a synoptic-scale cold front. In these studies the radar data are compared to conventional meteorological data obtained from the WKY tower facility for the purpose of radar data interpretation. It is shown that the acoustic radar echoes reveal the boundary between warm and cold air and other areas of turbulent mixing, regions of strong vertical temperature gradients, and areas of weak or no wind shear.

The third case study examines the relationship between the nocturnal radiation inversion and the low-level wind maximum or jet in the light of conclusions presented by Blackadar (1957). The low-level jet is seen forming well above the top of the inversion. Sudden rapid growth of the inversion occurs which brings the top of the inversion to a height equal that of the jet. Coincident with the rapid growth of the inversion is a sudden decrease in the intensity of the acoustic radar echoes in the inversion layer. It is suggested that the decrease in echo intensity reveals a decrease in turbulent mixing in the inversion layer as predicted by Blackadar. The observed wind speed and direction are seen to correspond very well with those predicted by the inertial oscillation theory suggested by Blackadar.

It is concluded that the acoustic radar can be a valuable tool for study in the lower atmosphere and suggestions are made as to possible uses.

17. KEY WORDS	18. DISTRIBUTION STATEMENT
Acoustic Sounding Boundary Layer Remote Sensing	CAT. 20

19. SECURITY CLASSIF. (of this report)	20. SECURITY CLASSIF. (of this page)	21. NO. OF PAGES	22. PRICE
Unclassified	Unclassified	89	$4.00

MSFC - Form 3292 (Rev December 1972)

For sale by National Technical Information Service, Springfield, Virginia 22151

ACKNOWLEDGMENTS

The author wishes to thank the Air Weather Service and the Air Force Institute of Technology for providing the opportunity and scholarship which made this study possible.

The author extends sincere gratitude to Dr. Rex L. Inman under whose guidance this research was done. His encouragement and interest were essential to the undertaking and completion of this study. Sincere appreciation is expressed to Professors Yoshikazu Sasaki and Frank Hall for their review of the manuscript and their helpful suggestions.

The author is deeply indebted to Jack Marks for his assistance and encouragement; to Charles Doswell whose ear was always open; and to Joe McFarland for placing a light at the end of the tunnel.

The personnel of the National Severe Storms Laboratory deserve a word of thanks for their interest in this research and for supplying the WKY tower data.

An expression of gratitude and love is extended to my wife, Ina, and my two daughters, Jennifer and Teresa,

for their patience and understanding through, though they will not admit it, a difficult time.

This research was done in connection with graduate study at the University of Oklahoma. This research was partially supported by the Atmospheric Sciences Section, National Science Foundation, NSF Grant GA-35403, and by the George C. Marshall Space Flight Center, contract NAS8-28659.

TABLE OF CONTENTS

LIST OF TABLES

LIST OF ILLUSTRATIONS

LIST OF SYMBOLS

A	antenna collecting area (m^2)
C	the speed of sound ($m\ sec^{-1}$)
C_T	temperature structure constant ($^\circ K\ cm^{-1/3}$)
C_v	velocity structure constant ($m\ sec^{-1}\ cm^{-1/3}$)
D	air column depth
D_T	temperature structure function ($^\circ K^2$)
D_v	velocity structure function ($m^2\ sec^{-2}$)
f	Coriolis parameter (sec^{-1})
k	wave number of the acoustic wave (cm^{-1})
L	an attenuation factor
P	transmitted acoustic power (w)
P_r	received acoustic power (w)
r	distance (cm)
R	range (m)
t	time
T	temperature ($^\circ K$)
v	wind speed ($m\ sec^{-1}$)
V_a	vector difference between the geostrophic and real wind

V_g geostrophic wind

V_{max} predicted maximum wind

V_r real wind

$V(t)$ predicted real wind at time t

Γ_d dry adiabatic lapse rate

ζ relative vorticity (sec^{-1})

θ direction acoustic power is scattered measured from the initial direction of propagation

λ transmitted wave length (cm)

σ scattered power per unit volume per unit incident flux per unit solid angle in the backscatter direction

$\sigma(\theta)$ scattered power per unit volume per unit incident flux per unit solid angle at angle θ from the initial direction of propagation

τ transmitted pulse length (sec)

ACOUSTIC SOUNDING IN THE PLANETARY BOUNDARY LAYER

CHAPTER I

INTRODUCTION

In recent years it has become increasingly evident that a better understanding is needed of the physical processes which are active in the planetary boundary layer. This need is especially apparent in the areas of low-level cloud prediction, severe weather forecasting, and the prediction of air pollution transport. The study necessary for better understanding of these complex processes has been seriously hampered by the lack of available data. In the past, direct sensing methods such as aircraft, instrumented towers, and balloon-borne packages have been used to obtain data from the boundary layer. All of these methods are expensive and, to varying degrees, disturb the field in which measurements are being made. Thus, it has been difficult to obtain the quantity and quality of data needed for meaningful study. The search for a solution to the problem of data collection

in the lower atmosphere has led meteorologists to remote sensing.

The chief advantage of a remote sensing instrument is its ability to gather information from regions here-to-fore inaccessible or, at best, difficult to reach. The observations are made remotely, without requiring that the instrument be placed in the region from which information is desired. With remote sensing there is no disturbance or modification of the field from which data are being collected.

Of the remote sensing instruments developed in recent years the most promising as a tool for boundary layer study is the acoustic radar. Because the atmosphere is the transmitting vehicle for sound waves, the acoustic radar is highly sensitive to fluctuations in both temperature and velocity, much more so than remote sensors employing electromagnetic waves. The acoustic radar can therefore be constructed from relatively simple equipment which results in a low initial cost compared to alternative sounding methods. The acoustic radar can provide continuous high-resolution observations automatically and inexpensively.

That the propagation of sound is affected by atmospheric conditions has been known for hundreds of years. Digges (1555) stated that bells being heard farther than

usual foretells of rain. However, no scientific study of sound waves and their interaction with the atmosphere was made until 1873. Tyndall (1875), while testing the audible range of various fog warning devices, found that the distance at which the same sound could be heard varied greatly from day to day. This variation was especially noted on days of similar visually observed atmospheric conditions. Tyndall also noted that while the sound became inaudible at some distance from its source, it was often heard again at some greater distance. He concluded that, at times, there existed concentric regions around the sound source in which the sound was alternately audible and inaudible.

In the laboratory Tyndall constructed a tube in which he placed platinum wires. A small bell was placed at one end of the tube; a flame, sensitive to the slightest disturbance of the air, at the other. When the platinum wires were heated, the flame was not disturbed by the sounding of the bell. Tyndall concluded that the temperature fluctuations of the air in the tube could attenuate the direct propagation of sound and lead to backscattering. He attributed the scattering of sound in the atmosphere to invisible "acoustic clouds...incessantly floating or flying through the air". After Tyndall's initial investigation, over 70 years passed

before the technique was studied again as an atmospheric probe.

In 1944, Gilman et al. (1946) used acoustic backscatter to study low-level temperature inversions and their effects on the propagation of microwave communications. An unexpected amount of atmospheric structure under the inversions was detected by acoustic sounding, and a strong correlation was noted between the acoustic inversion echo and microwave fading. The conclusions reached were that the backscattered acoustic energy was the result not only of strong temperature gradients but also, of turbulent temperature fluctuations, and that these fluctuations were the primary cause of backscattering. The breakup of nocturnal inversions and the formation of daytime thermals were also observed.

The first step in the evolution of acoustic sounding as a tool for meteorologists occurred in 1967. An acoustic sounding experiment was set up in Australia to study the temperature structure of the lower atmosphere and its relation to abnormal propagation of radio waves. The preliminary results of this experiment were reported by McAllister (1968). It demonstrated that a continuous record of the height, movement, and spatial distribution of inhomogeneities in the temperature structure of the lower atmosphere could be obtained

by acoustic sounding. Later McAllister et al. (1969) presented a detailed report of this experiment. Various meteorological phenomena were examined such as thermal plumes, radiation inversions, and breaking waves. This experiment confirmed that turbulent temperature and velocity fluctuations are the primary scatterers of acoustic energy. It was demonstrated that it is possible to separate the contributions to the scattered energy made by the temperature fluctuations and by the velocity fluctuations by operating the acoustic radar in the inclined monostatic and bistatic mode (Fig. 1).

In a study of thermal plumes and nocturnal inversions Beran et al. (1971) used acoustic sounding equipment to determine vertical velocities. By observing the Doppler shift in frequency of the backscattered acoustic signal they calculated detailed vertical velocity patterns, accurate to $\pm$ 0.2 m sec^{-1}. They demonstrated the potential of the acoustic Doppler shift as a means to gain new insight into such problems as low-level heat flux and the structure and motion of wave phenomena.

In one of the most recent studies Cronenwett et al. (1972) have suggested that the acoustic radar may be useful in predicting the formation and dissolution of low-level

stratus clouds. They also found that the acoustic radar is capable of detecting and measuring the velocity of small particulate matter in the air. These measurements will be of interest in the study of pollution diffusion. Marks (1972) has suggested another application of the acoustic radar to air pollution meteorology. In observing nocturnal inversions he found that the acoustic radar data reveal areas of strong temperature gradients, areas of turbulent mixing, and the exact time of inversion breakdown. Marks also found that the amount of fine structure revealed by the acoustic radar record cannot be attained by conventional instruments.

The purpose of this research is threefold; to add to the knowledge of pattern recognition and interpretation of acoustic radar data; to demonstrate the usefulness of the acoustic radar as a tool for meaningful study of the lower atmosphere; and to gain knowledge of the processes in action in the boundary layer. Two areas of interest have been investigated. First, a study was made of acoustic radar data collected during the passage of a mesoscale cold-air intrusion and a weak cold front. Results are presented as case studies relating the synoptic situation obtained from conventional teletype and facsimile data, the acoustic radar record, and time sections of temperature, wind speed, and wind

direction obtained from the meteorologically instrumented WKY television tower. In these case studies, attention is focused on the interpretation of the acoustic radar data.

In the second area of interest, attention is aimed at the relationship between the nocturnal temperature inversion and the low-level wind maximum. The WKY tower data are discussed in the light of theory presented by Blackadar (1957) on the interactions of these phenomena. In the presentation of the results of this study, the acoustic radar data will play an important supportive role.

CHAPTER II

ACOUSTIC RADAR THEORY

Transmission of acoustic energy into the atmosphere may result in reflection, absorption, or scattering. Reflection occurs when the acoustic energy encounters sharp gradients in the mean air temperature. Atmospheric absorption reduces the effective range of the radar by decreasing the amount of energy available for reflection or scattering. Absorption varies directly with the transmitted frequency and the relative humidity of the air and inversely with the temperature. Scattering of acoustic energy is caused by turbulent fluctuations of both wind velocity and temperature. Variations of water vapor pressure also cause scattering of acoustic energy. However, calculations made by McAllister et al. (1969) indicate that the effects of water vapor are below the threshold of detectability of present equipment.

The theory of the scatter of acoustic energy in dry air has been presented by Monin (1962). For a Kolmogorov

spectrum of turbulence, Monin's equation describing the scattering of sound reduces to (Little, 1969)

$$\sigma(\theta) = 0.03k^{1/3} \cos^2\theta \left(\frac{C_v^2}{C^2} \cos^2\frac{\theta}{2} + 0.13 \frac{C_T^2}{T^2}\right) \left(\sin \frac{\theta}{2}\right)^{-11/3}, \quad (1)$$

where $\sigma(\theta)$ is the scattered acoustic power per unit volume per unit incident flux per unit solid angle, at angle θ from the initial direction of propagation, $k = 2\pi/\lambda$ is the wave number of the acoustic wave, and C and T are the mean speed of sound and the mean temperature of the scattering volume. The values of C_V and C_T may be obtained from measurements of their respective structure functions given by

$$D_V = \overline{[v(x) - v(x+r)]^2} = C_v^2 \, r^{2/3},$$

and

$$D_T = \overline{[T(x) - T(x+r)]^2} = C_T^2 \, r^{2/3},$$

where v(x) and v(x+r) are the instantaneous wind speeds at the points x and x+r in the x to x+r direction and T(x) and T(x+r) are the instantaneous temperatures at x and x+r. Thus, C_v^2 and C_T^2 are, respectively, the mean square of the differences in velocity and temperature between two points separated by a unit distance.

Eq. 1 shows that: (1) acoustic energy is scattered

by fluctuations of both wind velocity and temperature; (2) both wind- and temperature-scattering terms are multiplied by $\cos^2\theta$; therefore, no acoustic energy will be scattered at an angle of 90° from the direction of propagation; (3) both scattering terms are multiplied by $(\sin\frac{\theta}{2})^{-11/3}$; hence, most of the acoustic energy is scattered into the forward hemisphere; (4) scattered acoustic energy varies weakly with the wave length; and (5) the wind term is multiplied by $\cos^2\frac{\theta}{2}$, which means all backscattered energy ($\theta = 180^\circ$) is the result of temperature fluctuations only.

Item 5 above is applicable to the present research. All acoustic radar data used in this study were collected by operating the radar in a vertically-directed monostatic mode (Fig. 1).

Considering only the backscattering of acoustic energy McAllister et al. (1969) have shown that, for isotropic homogeneous turbulence,

$$P_r = 0.5\ (PC\tau AL\sigma)\ R^{-2} \qquad (2)$$

where P_r is the power received (w), P is the transmitted power (w), τ is the transmitted pulse length (sec), A is the collecting area of the antenna (m^2), L is an attenuation factor which accounts for transducer and antenna efficiencies and atmospheric absorption, R is the range (m), and σ is the

scattered power per unit volume per unit incident flux per unit solid angle in the backscatter direction. The equation for σ is given as

$$\sigma = 0.008 \ (C_T^2 \lambda^{-1/3}) \ T^{-2}$$

where λ is the transmitter wave length (cm).

CHAPTER III

DESCRIPTION OF THE ACOUSTIC RADAR AND THE INSTRUMENTED TOWER FACILITY

The acoustic radar used in this research was constructed and placed in operation at the University of Oklahoma in 1971. Basically, the acoustic radar is a conventional pulsed radar which transmits a brief burst of acoustic energy. Backscattered and reflected energy is then received at some later time and displayed. Fig. 2 shows the functional block diagram of the radar and Table 1 lists the equipment parameters.

The cycle of operation begins at the facsimile recorder. When the recorder begins its trace across the paper, a synchronizing pulse is sent to the tone burst generator. This pulse allows the tone burst generator to pass a short burst of audio signal from the audio oscillator through a filter to the power amplifier. The amplified audio pulse is conveyed by transmission line to the transducer site. There the transmit-receive (TR) switch couples the audio pulse to

the driver which in turn produces vertically-directed sound. The TR switch provides a very important function. While in the transmit mode the TR switch disconnects the receiver section of the radar from the transducer. This prevents the high-power transmitted pulse from entering the receiver section and allows the transducer to be used as a transmitter and a receiving antenna.

A short time after transmission has begun, the sequence timer, activated by a pulse from the tone burst generator at the beginning of transmission, resets the TR switch to the receive mode. The sequence timer also initiates the generation of a voltage ramp which increases linearly with time during each cycle. The acoustic signal amplitude decreases as range increases. By multiplying the received acoustic signal by the voltage ramp, disturbances of equal amplitude, but at different heights, will be depicted as such.

The returning acoustic energy is converted to a voltage by the transducer and conveyed through the TR switch to the preamplifier. The returned signal then passes through the receiver and the amplifier to the multiplier. Here the voltage ramp is applied. The signal then passes through the recorder driver and on to the facsimile recorder where it is

displayed visually. This ends the cycle. The received signal may also be recorded on magnetic tape or displayed on an oscilloscope.

Since June, 1972, the University of Oklahoma acoustic radar has been in operation at a site near the meteorologically instrumented WKY television tower. The tower is located about 6 n mi north of Oklahoma City, Oklahoma. The terrain around the tower-radar site is gently rolling and covered with wild grass and weeds. The radar is situated about 450 m from the tower. The tower is 458 m tall and is instrumented at seven levels (23, 45, 90, 177, 266, 355, 444 m).

Horizontal wind speed, wind direction, and temperature are measured at all seven levels of the tower facility. Measurements of wind speed and direction are made with a Bendix Model 120 Aerovane. The wind speed sensor has a threshold speed of about 0.85 m sec^{-1}, a distance constant[1] of 5 m, and an accuracy of $\pm$ 0.25 m sec^{-1}. At each level an Aerovane is mounted 10 ft from the tower on a boom attached to the tower. The temperature measurements are made by a combination of two independent systems. The ambient system makes an absolute ambient temperature measurement at 23 and

---

[1]The distance constant is defined as wind passage by the propeller required for the anemometer output to reach 63% of a step speed change.

444 m. The delta system measures difference temperatures at all levels referenced to the ambient reading at the 444-m level. The sensors are linearized thermister composites housed in heat sink stainless steel probes, which are mounted in motor aspirated radiation shields. This shield reduces radiation heating effects to less than 0.11°C. The absolute accuracy of the thermistors has been found to be within 0.2°C. Each delta thermistor is calibrated to the reference thermister at the 444-m level, with the departure from the reference within $\pm$ 0.06°C.

The Gill propeller anemometer model 27100 is used to measure the vertical component of wind velocity at 23, 177, and 444 m. The threshold speed for this instrument is about 0.25 m sec^{-1} and its accuracy is better than 0.12 m sec^{-1}. At these same three levels the wet-bulb temperature is measured with a cloth-wrapped thermistor mounted in a motor aspirated shield. The cloth is kept moist by a capillary system.

Atmospheric pressure is measured at the base of the tower with a Belfort Model 6068 Microbarograph with a digital output. Changes in pressure are sensed by a bellows that transmitts its motion through a system of levers and gears to a low-torque potentimometer. A dc voltage is applied to the

potentiometer and its output is a dc voltage proportional to the pressure. The instrument has an absolute accuracy of $\pm$ 0.5 mb with a sensitivity of $\pm$ 0.2 mb.

The data collected by the tower instruments are recorded by two independent systems. The analog system records all wind, temperature, and pressure data on strip charts. The digital system records this data on magnetic tape. In this system each input channel is applied to a 100-channel scanner. The scanner sequentially scans through any preset number of channels from 1 to 100 at a rate of 200 channels sec^{-1}. The selected output of the scanner is digitized in a three-bit BCD word by an analog to digital converter. The digital data are then combined with time data in an IBM compatible format and written on magnetic tape.

The digital recording system is quite flexible and offers a wide choice of sampling rates and data record lengths. For rapidly changing weather conditions the system can scan and record all parameters at 2-sec intervals. The data used in this study were sampled at 1-min intervals.

A complete detailed description of the WKY tower facility has been reported by Carter (1970).

CHAPTER IV

INTERPRETATION OF ACOUSTIC RADAR DATA

To fully realize the capabilities and the potential usefulness of the acoustic radar, knowledge must be gained in the area of pattern recognition and interpretation of the radar data. It is to this end that these studies are presented.

The first case study examines in detail data collected during the passage of a shallow mesoscale cold-air intrusion. It is believed the cold air was thunderstorm outflow. Heavy thunderstorm activity had begun in southeastern Kansas in the early afternoon and had continued until shortly before midnight. It was from these thunderstorms that the cold air is thought to have originated. It was then carried by the ambient flow into central Oklahoma. In the second case, data collected during the passage of a shallow synoptic-scale cold front is examined.

It should be of interest here to make some comparisons on the observed structure and behavior of the mesoscale

cold intrusion and the synoptic-scale front. Both phenomena displayed a leading head[2] of cold air in the center of which was a core of coldest air. The leading head of the cold intrusion had a protruding nose, whereas, the leading edge of the cold front was almost vertical. This was more a function of wind speed as the intrusion was accompanied by stronger winds. On the leading edge of both the intrusion and the front, the horizontal temperature gradient was weakest at the surface. This was due to turbulent mixing with warmer ambient air. The cold front had overrun a portion of warmer surface air and was carrying it along. The temperature at the surface fell as the front passed but increased behind the front for a short time.

The wind structure of the two phenomena was quite similar except for the direction of the wind shift. There was the appearance of a layer of maximum winds above the surface in the cold air. This was especially noted in the case of the cold front. The front was made up of three separate surges of cold air. Each surge displayed a wind maximum. The wind shift in each case occurred at the surface before the cold air arrived. Above the surface the shift came with

---

[2]The term head, used here as an analogy to heads in laboratory gravity currents, describes the area at the front of the cold air mass where the depth of the cold air is greater than at points upstream.

the cold air. The most obvious difference in the wind structure is the direction of the wind shift. As the cold front passed, the wind direction changed in a clockwise sense (e.g., southwest to west to north). This was as expected for a synoptic-scale cold front. The wind shift accompanying the cold intrusion, although slight, was in the opposite sense. This difference was the major indicator that these two phenomena, although similar in many respects, were on different scales of atmospheric motion.

Case I

The surface synoptic situation for 0000 CST 21 June 1972 is shown in Fig. 3. A cold front which passed the Oklahoma City area 22 hrs earlier was located on a Lubbock-Dallas-Texarkana line moving southward at 8-10 kt. The front extended northeastward from Texarkana into the Chicago area. Winds behind the front throughout Oklahoma were from the northeast quadrant. A surface high pressure center was situated on the central Nebraska-South Dakota border. At the 850-mb level the cold front was about 20-30 n mi south of Oklahoma City; winds behind the front at that level were from the east-northeast. There was an area of scattered moderate thunderstorms along and behind the surface front in extreme southeastern Oklahoma, northwestern Texas, and southwestern

Arkansas. There was an area of light thunderstorms in northwestern Oklahoma and the northern Texas panhandle, and moderate rainshowers were occurring in southeastern Kansas. These rainshowers were the remains of the thunderstorm activity discussed earlier. Clouds over the site consisted of two broken layers, one at 12000 ft and the other at 25000 ft. The cloud cover remained unchanged between 0000 and 0800 CST.

At 0000 CST the air in the lower 450 m at the radar site was nearly isothermal with only a 1°C drop from the surface to the top of the tower (Fig. 4b). The wind speed increased rapidly from the surface to 175 m, then remained nearly constant above that level (Fig. 4d). Mixing caused by the strong vertical shear in the surface to 175 m layer combined with the temperature lapse rate less than dry adiabatic to produce turbulent temperature fluctuations. These fluctuations were recorded as backscattered acoustic energy on the radar record (Fig. 4a). The height of the recorded echoes corresponds closely with the height of the strong shear layer (Fig. 4d). Above 175 m the radar record indicates the absence of turbulent temperature fluctuations although the temperature profile in this region was much like that below 175 m, i.e., a lapse rate that was less than dry adiabatic. The weak vertical wind shear above 175 m yielded

this result. As shown by the radar record (Fig. 4a), this situation continued with little change until 0045 CST.

There was a gradual but slight increase in the depth of the strong shear layer between 0000 and 0045. This increase is more notable in the radar record than in the wind speed data from the tower (Fig. 4d). One can also see a raggedness in the height of the recorded echoes which cannot be seen in the analyses of the tower data. It must be pointed out here that the acoustic radar is recording a vertically continuous observation every four seconds and the tower instruments are sampling the parameters at one-minute intervals and are mounted at levels physically separated by as much as 89 m. The radar can, therefore, reveal fine structure which will not be found in the tower data. The black dots seen on the radar record at 0027, 0033, and 0042 CST at various heights are probably echoes from birds or large bugs. These observations are quite common.

At 0045 CST the cold intrusion passed the site. The passage was marked by decreasing temperature at all levels (Fig. 4b), a slight wind shift in the surface to 360-m layer (Fig. 4c), and an increase in wind speed (Fig. 4d). The horizontal temperature gradient across the leading edge of the cold air was strongest in the 250 to 350-m layer.

Surface friction apparently was retarding the advance of the cold air at the surface. The retardation resulted in a protruding nose on the leading edge of the cold air. Turbulent mixing of the cold air and the ambient air below the protruding nose had weakened the horizontal temperature gradient in this region (Fig. 4b). The temperature drop accompanying the cold intrusion arrived first and was sharpest at the level of the protruding nose.

The passage of the cold intrusion is quite notable on the acoustic radar record (Fig. 4a). At 0045 CST the appearance of the radar data changed abruptly. As the protruding nose cooled the layer between 250 and 350 m, the lapse rate from the surface to 350 m began to approach the dry adiabatic lapse rate. The temperature profiles for 0035 and 0051 are shown in Fig. 5. These profiles reveal the change which occurred as the nose of cold air passed the tower. The wind shear in the surface to 175 m layer weakened rapidly following the passage of the cold air (Fig. 4d). The dry adiabatic lapse rate and weak shear reduced the possibility of turbulent temperature fluctuations and hence produced an absence of echoes in the surface to 350 m layer (Fig. 4a). The turbulent mixing below the protruding nose can be seen as an area of weak echoes at the surface between

0045 and 0052 CST. The upper boundary between the ambient air and the cold air is marked by a layer of echoes approximately 100 m in depth. This resulted from both backscatter from turbulent mixing between the two air masses and reflection from the strong vertical temperature gradient at the 350-m level (Fig. 4b). The height of this strong vertical gradient decreased behind the upraised leading nose. This decrease in height is noted on the radar record (Fig. 4a) as the height of the echo layer began to lower shortly before 0100 CST.

After the cold air passed at the surface, the lapse rate from the surface to 325 m was no longer equal to but less than the dry adiabatic lapse rate. The temperature profile for 0107 is shown in Fig. 5. At this same time the wind speed in the lower 200 m became quite gusty and the wind shear in this layer increased (Fig. 4d). The resultant turbulent mixing is seen on the acoustic radar record as the bottom of the echo layer became quite ragged and echoes were seen near the surface. By 0115 the lapse rate below 180 m was again nearly dry adiabatic (Fig. 5) as cold advection at 180 m was stronger than at the surface. Although the wind shear continued strong and the wind speed gusty until 0138 (Fig. 4d) the lower ragged echoes disappeared from the

radar record at 0113 (Fig. 4a) in response to the dry adiabatic lapse rate.

On the leading edge of the cold intrusion the minimum temperature in the cold air was near 340 m. Upstream in the cold air the level of minimum temperature decreased. By 0130 CST the minimum temperature was at 250 m (Fig. 4b). Below this level the lapse rate was nearly dry adiabatic. Above 250 m a temperature inversion existed. Fig. 5 shows the temperature profile for this time. Upstream behind the protruding nose and just above the level of minimum temperature in the cold air was a layer of maximum wind speed (Fig. 4d). The wind speed maximum first appeared at 0116. At 0130 the vertical shear associated with the wind speed maximum and the inversion above 250 m produced a layer of echoes on the radar record from 250 to 450 m. By 0147 the level of minimum temperature had lowered to 235 m as the leading head of cold air passed the site (Fig. 4b). Preceding the arrival of the deeper cold air there was a broad region of upward vertical motion at the 444-m level with velocities on the order of 0.5 to 1.0 m sec^{-1}. At 23 m the motion was downward with velocities as high as 1.1 m sec^{-1} recorded. At 0147 the vertical wind shear was strong in the layer between 250 and 375 m (Fig. 4d). On the radar record (Fig. 4a) the

turbulent fluctuations caused by this layer of shear can be seen as the heavy layer of echoes between 250 and 375 m. Above 375 m there was an area relatively free of echoes. Here the vertical temperature gradient was weaker (Fig. 4b) as was the wind shear (Fig. 4d). The layer of weak echoes from 450 to 525 m marks the turbulent mixing at the boundary between the cold air and the ambient air.

Following the leading head of cold air downward vertical motion produced a broad thermal maximum centered at 0305 CST (Fig. 4b). The temperature profile at 0305 consisted of a less than dry adiabatic lapse rate from the surface to 225 m, the level of minimum temperature; a strong inversion from 225 to 365 m; and a neutral layer above 365 m. The level of maximum wind speed was 260 m (Fig. 4d). The acoustic radar record (Fig. 4a) revealed turbulent temperature fluctuations from the surface to 275 m; a layer of strong echoes from 275 to 325 m associated with the strong wind shear and strong vertical gradient of temperature in this layer; and a layer of weaker echoes from 325 to 365 m, where the shear and vertical gradient of temperature were slightly weaker than in the 275 to 325 m layer.

After 0305 CST the depth of the cold air and the height of the wind speed maximum began to increase. This

in turn caused an increase in height of the region of strong wind shear above the wind speed maximum (Fig. 4d) and of strong vertical temperature gradient between 275 and 365 m (Fig. 4b). This increase in height was strikingly displayed on the acoustic radar record (Fig. 4a). The layer of strong shear and strong vertical temperature gradient is seen as a layer of strong echoes which had separated from the lower region of echoes and was gradually increasing in height. By 0350 this layer was between 350 and 450 m. The heights are verified by the acoustic echoes (Fig. 4a), the temperature data (Fig. 4b), and the wind speed analysis (Fig. 4d). The echo-free region between 300 and 350 m, at first look, indicated a weakening of the wind shear and vertical gradient of temperature in this layer. Closer inspection of this region revealed an almost total absence of wind shear across the wind speed maximum. The temperature profile of this region, a weak inversion, would enhance the possibility of turbulent fluctuations of temperature. The absence of echoes in this region, and hence the absence of turbulent fluctuations, implies a lack of vertical shear across the wind speed maximum. The level of maximum winds had become a layer of maximum winds with an almost constant speed through the layer. The depth of the layer of nearly constant wind speed is seen

as the depth of the echo-free region on the radar record (Fig. 4a).

After 0400 CST the layer of maximum winds continued to increase in height (Fig. 6d) as the cold air deepened. The layer also deepened as indicated by the increased depth of the echo-free region on the radar record (Fig. 6a). At 0430 the echo-free region extended from 350 to 525 m. The layer of echoes from the surface to 350 m continued to show the result of shear below the layer of maximum winds and the lapse rate less than dry adiabatic. These echoes had weakened somewhat, especially those between 200 and 350 m. By 0500 the echoes had all but disappeared in the 200 to 350 m layer (Fig. 6a). The echoes were still strong below 200 m and weaker echoes were seen at 650 m. The latter echoes were the continued backscatter from the turbulent mixing in the region of strong shear above the layer of maximum winds. There seems no apparent reason for the disappearance of the echoes from the 200 to 350 m layer. The lapse rate in this region was still less than dry adiabatic (Fig. 6b) and the vertical wind shear was unchanged (Fig. 6d). A possible explanation is that the analysis of the wind speed data is incorrect. This analysis was done without consulting the acoustic radar record. The wind shear seen at 0500 between

the 177-m and 266-m tower data collection levels may have been concentrated near the 177-m level with less shear above 200 m. By 0530 it can be seen that the wind shear in the region had weakened (Fig. 6d).

The passage of the elevated head of cold air at 0147 and the strong downward motion behind the head created a gravity wave upstream in the cold air. This wave motion was quite notable in all parameters from 0550 to 0800. The wind direction (Fig. 6c) showed some periodic change although it was slight compared to the periodicity revealed by the wind speed (Fig. 6d) and the temperature data (Fig. 6b). The wind speed maximum responded to this wave motion by oscillatory changes in height. This produced alternating regions of upward and downward vertical motion. Vertical velocities as high as 1.4 m sec^{-1} were recorded during this period. The alternating vertical motion in turn caused alternating regions of cold air due to rising motion and regions of warm air due to subsidence. This large scale oscillation in all parameters is quite obvious from the analyses and a detailed discussion is not needed. Attention must be drawn, however, to the higher frequency wave motion superimposed on the long wave. This short wave motion was most notable in the wind speed analysis (Fig. 6d). One can easily see this between 0645

and 0655 as the short wave trough coincided with the long wave ridge. Again between 0700 and 0718, the short wave motion was very apparent. The wind direction also responded to the short wave motion (Fig. 6c). The direction became quite erratic after 0613, about the same time the wind speed began to reflect this motion.

The acoustic radar record also revealed both the long and short wave motion (Fig. 6a). The long wave motion was quite obviously displayed as the periodic height changes of the echo layer. The height of the echo layer was gradually increasing during the period from 0550 to 0800 but the wave motion can be seen superimposed on this rising trend. The period was on the order of one hour, the same noted in the analyses of the tower data. The short wave motion is clearly seen, especially between 0645 and 0710, as oscillations within the layer of echoes. No more discussion of the radar record is needed here save the cause of the echoes.

At 0545, about 30 min after sunrise, the surface began to warm. This warming resulted in a layer of air at the surface in which the lapse rate was dry adiabatic. As this layer deepened the relatively echo-free region at the surface deepened (Fig. 6a). The cause of the layer of echoes seen on the record may be best seen by selecting a few points

in time and examining the data at these points.

At 0620 the layer of echoes appeared between 100 and 200 m (Fig. 6a). The temperature profile for 0620 (Fig. 7) shows the lapse rate was nearly dry adiabatic from the surface to about 100 m. Above, it was less with an inversion between 180 and 350 m. On the wind speed analysis (Fig. 6d) one can see the stronger wind shear from the surface to 200 m. The echoes between 100 and 200 m were caused by turbulent mixing of the air in the region where the lapse rate was less than dry adiabatic.

At 0646 the lapse rate was dry adiabatic from the surface to 310 m (Fig. 7). This was caused not only by the sun's warming at the surface but also by the formation of the cold air pocket centered at 310 m (Fig. 6b). The echo-free area had deepened to about 250 m (Fig. 6a). The echoes were also stronger than those seen at 0620. This increased intensity was caused by the sharp vertical gradient of temperature above the pocket of cold air. By 0725 the bottom of the layer of echoes was lower as the warming by subsidence above 150 m rendered the lapse rate above that height less than dry adiabatic (Fig. 7). The echoes became much weaker here as there no longer existed any region of strong vertical temperature gradient (Fig. 6a).

At 0745 a repeat of the 0646 conditions can be seen. ıe wind shear in the region of the strong vertical temperature gradient above the cold air pocket was not as strong as seen at 0646, but the temperature gradient was strong and the reflected energy resulted in another region of stronger echoes.

Case II

At 1700 CST, 4 August 1972, a cold front, oriented northwest to southeast and moving southward at 8-10 kt, lay across Oklahoma (Fig. 8). South of the front ceilings ranged from 8-10000 ft broken in southwestern Oklahoma to 25000 ft broken in the southeastern and southcentral sections of the state. There were some widely scattered rain showers in central Oklahoma. Winds south of the front were from the south at 5-10 kt except in the vicinity of the showers. Immediately behind the front winds were from the northwest but shifting gradually to the northeast about an hour after frontal passage. Circulation around a surface high pressure center located over northern Illinois was dominating the flow behind the front. Ceilings behind the front in Oklahoma were 25000 ft broken. Further north in Kansas, low stratus, with ceilings as low as 500 ft overcast, fog, and drizzle were common. There were rain showers in southwestern Missouri,

and heavy rain and fog in northwestern Arkansas. At the 850-mb level (Fig. 9) winds from the south were bringing warm moist air into the Oklahoma area.

At 1700 a rain shower was in progress over the acoustic radar site. The effect of rain falling on the radar antenna can be seen in the acoustic radar data collected from 1700 to 1735 (Fig. 10a). The rain began at 1700 and the air cooled rapidly at all levels during the rain (Fig. 10b), and the wind speed was quite gusty (Fig. 10d). From the radar record it can be seen that the rain was alternately heavy then light and ended at 1735. The air warmed and the wind speed dropped to almost calm at the surface after the shower ended.

The cold front passed the WKY tower at 1806 CST. The leading edge of the cold air mass was almost vertical. This was quite dramatically displayed by the acoustic radar (Fig. 10a). The depth of the leading edge was about 525 m. The cold air boundary is shown by the dark echoes resulting from the turbulent mixing between the cold air and the warmer ambient air. The temperature drop associated with the front was sharpest at 350 m and quite weak at the surface (Fig. 10b). This was indicative of turbulent mixing at the surface which had lessened the temperature gradient through the

front. This mixing was probably the cause of the echoes seen near the surface for several minutes following the leading edge of the front (Fig. 10a). The boundary of the previously discussed portion of warm air being carried along by the front may be seen as the light echoes at the surface between 1805 and 1810.

The wind shift associated with the front arrived at the surface several minutes before the temperature decrease occurred (Fig. 10c). A wind speed minimum accompanied the wind shift at the surface (Fig. 10d). At the upper levels the wind shift, wind speed minimum, and temperature decrease arrived almost simultaneously. Immediately behind the passage of the cold air a wind speed maximum occurred at all levels.

Upward vertical velocities on the order of 0.7 to 1.2 m sec^{-1} were recorded at 444 m prior to the arrival of the leading head of cold air. Behind the leading head downward vertical motion occurred with velocities as high as 1.7 m sec^{-1} recorded. The subsidence behind the leading head resulted in a temperature increase at all levels. This thermal maximum was centered at 1816 (Fig. 10b). The acoustic radar reflected this downward motion as a decrease in the height of the echo layer at 1816 (Fig. 10a). As the cold

air deepened again, upward motion was again noted at the 444-m level. The velocities ranged from 0.4 to 1.4 m sec^{-1}. The second head of cold air was equal in depth to the first and following its passage the echo layer decreased again.

At 1850 a second surge of cold air arrived with the minimum temperature core at 180 m (Fig. 10b). This was accompanied by a slight increase in wind speed (Fig. 10d). The boundary of the colder air can easily be seen on the radar record as an increase in the height of the echo layer just prior to 1900 (Fig. 10a). The depth of the colder air was about 375 m. The depth was verified by the tower temperature data as the 355-m level sensor recorded a slight temperature decrease at this time while the temperature at 444 m remained unchanged. Behind the surge of cold air, downward motion resulted in warming (Fig. 10b). Downward vertical velocities as high as 2.0 m sec^{-1} were recorded at 177 m following the passage of the deeper mass of cold air. The horizontal wind speed decreased behind the cold surge (Fig. 10d).

Following the surge of cold air, the cold air became quite shallow and very nearly lost its identity on the acoustic record (Fig. 10a). The cold air was being mixed with warmer ambient air to the point that by 1930 only a

very thin layer of cold air remained on the surface. Above this existed a deep boundary of mixed air. This continued until the arrival of another surge of cold air at approximately 2006.

This third surge of cold air was, like the second, most pronounced at the 177-m level (Fig. 10b). But, unlike the second, it was noted at all levels of the tower as the depth of this surge was about 500 m. The cold air was accompanied by an increase in wind speed at all levels (Fig. 10d). The increase was most notable in the layer from 100 to 230 m, corresponding roughly to the layer of most pronounced temperature change. The speed increase was least at the surface and the top of tower. The wind shift was most pronounced at the 444-m level however (Fig. 10c). The wind at and near the surface had been gradually shifting toward the east following the initial rapid shift accompanying the front. At the upper levels of the tower the winds had shifted back to the southwest following the passage of the deep leading head of cold air. Therefore, the arrival of another deep layer of air caused a more pronounced wind shift at 355 and 444 m.

The arrival of the third surge of cold air was noted on the radar record at 2006 (Fig. 10a). The boundary of mixing cold and warmer ambient air extended to about 500 m.

This surge had an upraised leading nose followed by a deeper, colder head. This is seen very clearly in the temperature analysis (Fig. 10b) as well as the acoustic radar record. It's appearance is somewhat similar to the leading edge of the cold intrusion discussed in Case I of this section. Turbulent mixing was again seen near the surface below the leading nose of cold air.

Following the last surge of cold air, the cold air again became shallow and soon lost its identity as the warmer air above mixed with it. Evidence of mixing at the surface lasted until a few hours after sunrise.

CHAPTER V

NOCTURNAL LOW-LEVEL WIND MAXIMUM

The vertical profile of horizontal wind speed sometimes shows a relatively sharp peak or "nose" within the lowest 1500 m of the atmosphere. This thin layer of maximum wind speed is generally known as the "low-level jet". Wind speeds in the jet are often twice those found a few hundred meters below or above. The low-level jet has been observed in all parts of the United States, in all seasons, and at all hours of both day and night (Bonner, 1968). However, the low-level wind maxima achieve greatest development and occur most frequently in the central and southern plains areas of the United States during the summertime between midnight and sunrise. The most frequently observed direction is southerly.

The low-level jet is of great interest to meteorologists because of the indirect evidence which may be inferred about turbulent mass transport in the lower atmosphere and because of the apparent relationship between the jet and the high frequency of nocturnal thunderstorms in the plains area

of the United States. The phenomenon is also of practical interest. The low-level jet has proven to be very hazardous to aircraft landing operations. The strong vertical shear below the layer of maximum wind speed results in a rapid loss of airspeed for a descending aircraft. This can be especially dangerous for jet aircraft which normally land at near-stall speeds. The low-level jet is also known as a fuel or time saver for the pilot of the small private airplane. One such pilot reported flying from New Orleans to Cleveland via Joliet, a distance of 1180 mi, in a plane with a range of only 1050 mi (Durosko, 1962).

There have been several theories proposed for the formation of the low-level wind maximum. Blackadar (1957) suggested that the boundary layer winds, which include the low-level jet, undergo a diurnal oscillation similar to the theoretical inertial oscillation (see Hess, 1959, 170-172). During the day the real wind is a balance between the pressure gradient, Coriolis, and frictional forces. Near sunset a radiation inversion forms at the surface. The air above the inversion layer, no longer being mixed with the air in the inversion layer, is essentially decoupled from the frictional force and is allowed to accelerate. It is accelerated by the rotation of the ageostrophic vector (V_a in Fig. 11a),

the vector difference between the geostrophic wind (V_g in Fig. 11a) and the real wind (V_r in Fig. 11a). The maximum boundary-layer speed during the night is related to the magnitude of the ageostrophic vector at the time of decoupling. At its maximum the wind speed would be equal to the geostrophic wind speed plus the magnitude of the ageostrophic vector. The period for one complete oscillation is one-half pendulum day and the wind speed reaches its maximum about 6 pendulum hours after sunset. Since the magnitude and direction of the real wind approach those of the geostrophic wind as the height increases, the largest ageostrophic vector, and hence, the greatest acceleration, would occur at or just above the top of the radiation inversion (Fig. 11b). It is at this level the low-level jet would appear.

Another prominent theory, proposed by Wexler (1961), involves the turning northward along the Central American mountains of tradewind air that enters the Gulf of Mexico. Wexler proposed a two-layer model, the upper layer stationary, the lower flowing northward below 2 km. This air moving northward provides the volume used by the high-speed low-level jet. The principle of the jet is explained by the conservation of potential vorticity. If $(f + \zeta)/D$ is constant for air columns moving northward and if D, column thickness, remains

constant, then as f, the Coriolis parameter, increases with increasing latitude, the columns of air must take on increasing anticyclonic relative vorticity, ζ. If this is converted to anticyclonic shear, then a high-speed flow must develop on the western boundary of the north-moving layer. Friction along the high plains and Rocky Mountains would cause strong shear of the opposite sense on the western side of the flow, resulting in the appearance of a true jet in the horizontal. Friction at the surface would cause vertical wind shear in the lower layer. This combined with the stationary layer above 2 km would give the flow a jet-like appearance in the vertical. As radiation alternates to create and destroy the surface nocturnal inversion, the vertical frictional stresses would undergo a strong diurnal variation, and so change the vertical profile of the jet.

There are strong and weak points in both of the theories described above. Wexler's theory implies the jet would be in action both day and night, with some variation caused by surface friction during the day, and that the low-level wind maxima have a jet-like appearance in the horizontal as well as the vertical. Hoecker (1963) found the jet does often persist during the day and does exhibit a wind speed maximum in the horizontal. Wexler's theory,

however, puts a limit on the direction of the jet, southerly, and calls the Rocky Mountains the western boundary of occurrence. Bonner (1968) showed that southerly is the most common, but clearly not the only direction from which the jet has been observed. Studies made by Rider and Armendariz (1966, 1971) indicate that the low-level jet occurs west of the Rockies. Blackadar's theory implies that the formation of the jet depends on the formation of the nocturnal radiation inversion. It has been found that the jet can occur when the temperature profile is dry adiabatic (Hoecker, 1963) and that the nocturnal inversion may occur without the formation of the low-level jet. Blackadar's theory is strengthened by the fact that most occurrences of the low-level jet are in the night time hours and are accompanied by a surface radiation inversion with the top of the inversion below or at the level of maximum wind speed (Bonner, 1968; Rider and Armendariz, 1971).

It is not the purpose of this research to examine either the formation of the low-level jet or the merit of any theory on its formation, but rather to investigate the relationship of the jet to the nocturnal inversion in the light of conclusions reached by Blackadar (1957). In the presentation of his theory, he dealt at some length on the

relationship of the two phenomena. Above the height of about one meter, the rate of nocturnal cooling is too large to be accounted for by radiational or conductive fluxes. It is therefore evident that turbulent transfer is the chief control on the rate of upward propagation of the inversion surface. The cause of the turbulence lies in the strong wind shear which develops within the inversion and which supplies the turbulent energy to overcome stability. When stability is overcome the inversion may be destroyed, deepen in a chaotic fashion, or grow slowly and orderly upward. The character of the wind profile will determine which alternative will occur.

Blackadar concluded that if the wind speed maximum is some distance above the top of the inversion, the inversion will either be destroyed or grow upward chaotically. However, while the wind shear is probably strong enough to allow a continual generation of turbulence, the presence of the wind speed maximum at the top of the inversion assures that the generation of turbulence is kept under control. The inversion will grow upward slowly and orderly, with the height of the wind speed maximum increasing slowly to remain coincident with the top of the deepening inversion. The existence of a jet-like profile with a wind maximum at the

top of the inversion is a stable configuration according to Blackadar.

In a study of low-level jet occurrences over White Sands Missile Range, Rider and Armendariz (1971) found that the height above ground of the wind speed maxima and the magnitude of the wind speed are erratic or fluctuate with time when the nose of the speed profile is well above the temperature inversion. Air Force pilots flying low-level missions have often reported strong turbulence near a low-level jet, while pilots flying the same route a short time later report no turbulence but the continued existence of the strong winds (McFarland, 1973). These findings indicate that the occurrence of the jet well above the top of the inversion is not a stable configuration and that the jet occurs, at times, without the turbulence suggested by its strong wind shear. These findings tend to add some support to Blackadar's conclusion that the coincidence of the wind speed maximum and the top of the inversion is stable and the generation of turbulence is under control. It is with this conclusion in mind that this case study is presented.

The synoptic situation for the night of 31 July-1 August 1972 was quite favorable for the formation of the low-level jet. The surface analysis for 0000 CST 1 August

(Fig. 12a) shows southeasterly winds prevailed over Oklahoma around a low pressure center in southwestern New Mexico. A similar pattern existed at the 850-mb level 6 hrs earlier (Fig. 12b). Sky conditions over the state ranged from clear to thin scattered cirrus.

About 40 min before sunset, which was 1935 CST, a weak inversion formed in the lower 50 m at the radar site. This occurrence is quite common in central Oklahoma (Goff and Hudson, 1972). After sunset the inversion intensified rapidly and began to deepen. By 2200 CST the inversion extended to about 200 m, strongest between the surface and about 50 m (Fig. 13b). The wind speed analysis for 2200 (Fig. 13c) shows that strong vertical shear existed in the inversion layer. Turbulent mixing caused by the shear was revealed by the acoustic radar (Fig. 13a). The strong echoes indicate that turbulent mixing existed throughout the inversion layer.

By 2330 the rapid cooling at the surface and the resultant shrinkage of the lower 50-75 m of the atmosphere had produced subsidence warming at about 75 m. This resulted in a double inversion temperature profile from the surface to 220 m. The depth of the inversion layer had gradually increased between 2200 and 2330 and was continuing to do so.

This was most easily seen on the acoustic radar record as an increase in the depth of the echo layer (Fig. 13a). By 2330 the wind speed had begun to increase with a definite speed maximum at about 290 m (Fig. 13c). Fig. 14 shows clearly that the wind speed maximum was located about 70 m above the top of the inversion layer.

Shortly after 0000 CST a rapid increase in the depth of the echo layer and an equally rapid decrease in echo intensity was seen in the acoustic radar data (Fig. 13a). The temperature analysis (Fig. 13b) reveals that the inversion had suddenly deepened up to the level of the maximum wind speed (Fig. 13c). The temperature at the level of maximum wind speed remained relatively unchanged and it was this temperature which became the top of the inversion after the rapid change. Richardson numbers calculated for the layer from 50 m below to 50 m above the inversion were above the critical value for instability of 0.25 until 2352. Richardson numbers were intermittently below 0.25 between 2352 and 0002; less than 0.25 between 0003 and 0013, the period of rapid change; and intermittently below 0.25 after 0013. The cause for the decrease in the value of the Richardson numbers was the increase in vertical wind shear below the level of maximum winds (Fig. 13c). Apparently, the shear below the wind

maximum became strong enough to overcome the stability of the inversion. The resulting turbulence mixed the air below the jet and destroyed the inversion at 220 m. The rapid change in the temperature profile can be seen in Fig. 15.

Following the period of turbulent mixing, the top of the inversion was at the same level as the maximum wind speed. The speed and temperature profiles for 0032 are shown in Fig. 16. This configuration is stable according to Blackadar (1957) and the generation of turbulence should be under control. Although the shear below the wind maximum remained strong (Fig. 13c), the reduction in the intensity of the acoustic radar echoes after 0005 (Fig. 13a) may indicate that turbulent mixing did decrease following the relocation of the top of the inversion so that it became coincident with the level of maximum wind speed.

There are two questions which must be answered at this point. First, does this observed wind maximum meet the criteria for the low-level jet set forth by Blackadar? He referred to a significant wind maximum as one in which the wind speed reaches a maximum within the first 1.5 km above the ground and then decreases by at least 2.5 m sec^{-1} to the next higher minimum. The height of the wind maximum in this study was about 290 m, well within the first 1.5 km of the

lower atmosphere. The magnitude at the maximum level at 2330 was about 15.5 m sec^{-1}. At the 444-m level of the tower the speed was 12.4 m sec^{-1} at 2330. If the next higher minimum was at the top of the tower, the wind maximum did meet the criterion. It is likely that the next higher minimum was much higher and the wind speed much less than 12.4 m sec^{-1} as the wind speed at the 850-mb level was on the order of 6-8 m sec^{-1}. This wind maximum also met the criteria set by Bonner (1968) to be classified as a low-level jet.

The second question involves the change in intensity of the acoustic radar echoes which occurred with the change in the depth of the inversion. Could some characteristic of the radar cause such a change? There are two possibilities here. If an acoustic wave is transmitted vertically into a layer in which the wind speed is increasing in height, the path of the wave will be curved. As the wave traveled higher, scattering volumes, which could result in backscattered energy, would be further removed horizontally from the vertical "aim" of the transmitter. Likewise the energy backscattered would return to the receiver in a curved path. A change in the wind profile, in speed or direction, over the radar site could result in a change in echo intensity as it would physically change the region into which the acoustic

energy is being transmitted. However, this change would have to be rather abrupt to cause an abrupt change in the radar data. As can be seen in Fig. 13c, there was no abrupt change in wind speed. The wind direction was constant at all levels of the tower throughout the period. The second possibility is a change in the scale of turbulent mixing. The acoustic radar is most sensitive to turbulent temperature fluctuations on the order of 10 cm. The breakdown of the inversion at 220 m may have caused the scale of fluctuations to change to a dimension to which the radar is not as sensitive. Hence, a change in the echo intensity would have occurred. As can be seen in Fig. 15, the breakdown of the inversion did not affect the temperature profile to any large degree below 150 m. But the intensity of the radar echoes did change in this region (Fig. 13a). This would indicate that this characteristic of the radar probably had little to do with the observed change of intensity.

If it can now be assumed that the decrease in echo intensity was caused by a decrease in turbulent mixing below the jet, this low-level jet-inversion occurrence fits quite well Blackadar's conclusion. The inversion began to form near sunset. Several hours later the jet formed above the top of the inversion. Strong wind shear caused turbulent

mixing in the inversion layer. The heavy layer of echoes on the acoustic radar record (Fig. 13a) gave some measure of that turbulent mixing. Then came the sudden increase in the height of the inversion layer up to the level of the jet. The jet speed continued to increase and the shear below the jet became stronger. But the turbulent mixing below the jet decreased, as revealed by the change in echo intensity on the radar record.

The top of the inversion and the jet remained at the same height, 290 m, until about 0315 CST, then, remaining coincident, began a slow increase in height to 450 m by sunrise. After sunrise the jet-inversion structure broke up.

To close out this case study, it should be of interest to compare the speed and direction of the observed jet with those of the jet predicted by Blackadar's inertial oscillation. To find the predicted wind, the real wind and the geostrophic wind are needed at the time of the decoupling described earlier. The surface inversion formed at 1855 CST; sunset occurred at 1935. The average of these times, 1915, was taken as an estimated time for decoupling. The surface geostrophic wind speed, 11.5 m sec^{-1}, was computed from 1900 CST surface observations. The direction, 178°, was estimated from the surface analysis for 1900.

The real wind speed, 8.5 m sec^{-1}, and direction, 151°, were the averages of a 10-min period of data, centered at 1915, from the upper three levels of the tower, 266 355, and 444 m. These three levels were chosen because the jet was observed between 290 and 450 m. The real and geostrophic winds (V_r and V_g, respectively, in Fig. 17) were plotted and the ageostrophic vector (V_a in Fig. 17) was determined. Fig. 17 shows the valid time, direction, and speed of the winds predicted by the inertial oscillation. Note that the maximum wind was predicted to occur at 0308 CST, from 178°, and with a speed of 16.0 m sec^{-1}. Predicted winds for other times may be found by interpolating along the circle to the disired time, measuring the length from the origin to that point, ¼" = 1 m sec^{-1}, and measuring the angle as indicated (Fig. 17).

Fig. 18 shows the speed and direction of the real winds. These were plotted from the tower data. They represent the speed and direction of the maximum wind recorded for the time given. The highest wind speed recorded during the night was 17.5 m sec^{-1}, from 172°, at 0323 CST, very close on all measures to the maximum predicted (Fig. 17). It should be noted that the observed winds followed the predicted pattern more closely after 0000 CST than before, or

after the top of the temperature inversion became coincident with the low-level jet.

CHAPTER VI

SUMMARY AND CONCLUSIONS

The acoustic radar proved to be a valuable asset to the study of the planetary boundary layer at the very outset of this research. The low-level jet-nocturnal inversion observed 31 July-1 August 1972 occurred when the conventional synoptic information indicated little of interest was taking place. The WKY tower data is much too voluminous for routine inspection. The acoustic radar record, however, can be examined daily in a matter of minutes. Examination of the radar data for the night of 31 July-1 August revealed that something had occurred that warranted investigation. The use of the acoustic radar as a monitor of the lower atmosphere could be very important.

The case studies presented here suggest other important uses for the acoustic radar. As theory predicted, these studies confirmed that the primary sources of backscattered acoustic energy are turbulent fluctuations of temperature and strong temperature gradients. This being true, much can

be inferred about the temperature and wind structure of the lower atmosphere from the examination of acoustic radar data. The boundary between air masses of differing temperatures can easily be seen as was shown in the studies of the cold intrusion and the cold front. Changes in the height of such a boundary would yield qualitative information of the vertical motions along that boundary. This suggests that the acoustic radar should be a useful tool in the study of cold outflow from thunderstorms, fronts, thermal, and wave motion in the atmosphere. The indication of regions of strong wind shear on the acoustic radar data implies that the radar could be a valuable aid in aircraft operations, particularly in the case of light aircraft, to which strong shear is a definite hazard.

Although these studies and the above suggestions have been limited to qualitative interpretation of acoustic radar data, this does not imply that the acoustic radar is limited to qualitative data only. Determination of the structure constants of wind and temperature and the use of the Doppler shift of the acoustic returns would yield quantitative information on horizontal and vertical velocities and temperature.

The acoustic radar data was used in the study of the low-level jet occurrence not to suggest, but to demonstrate

the usefulness of the radar. This jet-inversion occurrence behaved almost exactly as predicted by Blackadar (1957). The acoustic radar clearly revealed the sudden rapid growth of the inversion, and after the inversion top and the jet became coincident, the radar may have indicated a decrease in the amount of turbulent mixing in the inversion layer below the jet. The decrease in turbulent mixing could not have been seen with conventional meteorological instruments. However, more study is needed in this area to determine the capabilities of the acoustic radar in the measurement of turbulent mixing.

Aside from the acoustic radar, this case study offers some insight into one of the most interesting of boundary layer phenomena. It suggests that, although the low-level jet does occur when other temperature profiles are observed, the preferred or stable configuration is one in which the temperature profile is somewhat similar to that of the wind speed, and that when this configuration is attained, the jet winds follow Blackadar's inertial oscillation closely. This conclusion must be viewed in the light of the fact that this was the study of only one such occurrence. Clearly, more study is needed in this area.

REFERENCES

Beran, D. W., C. G. Little, and B. C. Willmarth, 1971: Acoustic Doppler Measurements of Vertical Velocities in the Atmosphere. Nature, 230, 160-162.

Blackadar, A. K., 1957: Boundary Layer Wind Maxima and Their Significance for the Growth of Nocturnal Inversions. Bull. Amer. Meteor. Soc., 38, 283-290.

Bonner, W. D., 1968: Climatology of the Low Level Jet. Mon. Wea. Rev., 96, 833-850.

Carter, J. K., 1970: The Meteorologically Instrumented WKY-TV Tower Facility. National Severe Storms Laboratory, Tech. Memo. No. 50, 18 pp.

Cronenwett, W. T., G. B. Walker, and R. L. Inman, 1972: Acoustic Sounding of Meteorological Phenomena in the Planetary Boundary Layer. J. Appl. Meteor., 11, 1351-1358.

Digges, L., 1555: A Prognostication of Right Good Effect. London.

Durosko, T., 1962: Low-Level Jet Streams. Flying, 71.

Gilman, G. W., H. B. Coxhead, and F. H. Willis, 1946: Reflection of Sound Signals in the Troposphere. J. Acoust. Soc. Amer., 18, 274-283.

Goff, R. E., and H. R. Hudson, 1972: The Thermal Structure of the Lowest Half Kilometer in Central Oklahoma: December 9, 1966-May 31, 1967. National Severe Storms Laboratory, Tech. Memo. No. 58, 53 pp.

Hess, S. L., 1959: Introduction to Theoretical Meteorology. Holt, Rinehart, and Winston, New York, 170-172.

Hoecker, W. H., Jr., 1963: Three Southerly Low-Level Jet Systems Delineated by the Weather Bureau Special Pibal Network of 1961. Mon. Wea. Rev., 91, 573-582.

Little, C. G., 1969: Acoustic Methods for the Remote Probing of the Lower Atmosphere. Proc. I.E.E.E., 57, 571-578.

Marks, Jr. R., 1972: Acoustic Radar Investigation of Boundary Layer Phenomena. Master's Thesis, University of Oklahoma.

McAllister, L. G., 1968: Acoustic Sounding of the Lower Troposphere. J. Atmos. Terr. Phys., 30, 1439-1444.

McAllister, L. G., J. R. Pollard, A. R. Mahoney, and P. J. R. Shaw, 1969: Acoustic Sounding--A new Approach to the Study of Atmospheric Structure. Proc. I.E.E.E., 57, 579-587.

McFarland, M. J., 1973: Personal communication.

Monin, A. S., 1962: Characteristics of the Scattering of Sound in a Turbulent Atmosphere. Akusticheskij Zhurnal, Vol. 7, 457-461 (Sov. Phys. Acoust., Vol. 7, 370-373).

Rider, L. J. and M. Armendariz, 1966: Low-Level Jet Winds at Green River, Utah. J. Appl. Meteor., 5, 733-736.

Rider, L. J. and M. Armendariz, 1971: Nocturnal Maximum Winds in the Planetary Boundary Layer at White Sands Missile Range, New Mexico. J. Appl. Meteor., 10, 1154-1161.

Tyndall, J., 1875: Sound. Appleton Co., London, 3 ed., Ch 7.

Wexler, H., 1961: A Boundary Layer Interpretation of the Low-Level Jet. Tellus, 13, 369-378.

Table 1

Acoustic Radar Parameters

Range	700 meters
Frequency	1500 Hertz
Acoustic Pulse Power	30 watts
Pulse Length	42.6 milliseconds
Receiver Bandwidth	70 Hertz
Antenna Diameter	1.21 meters

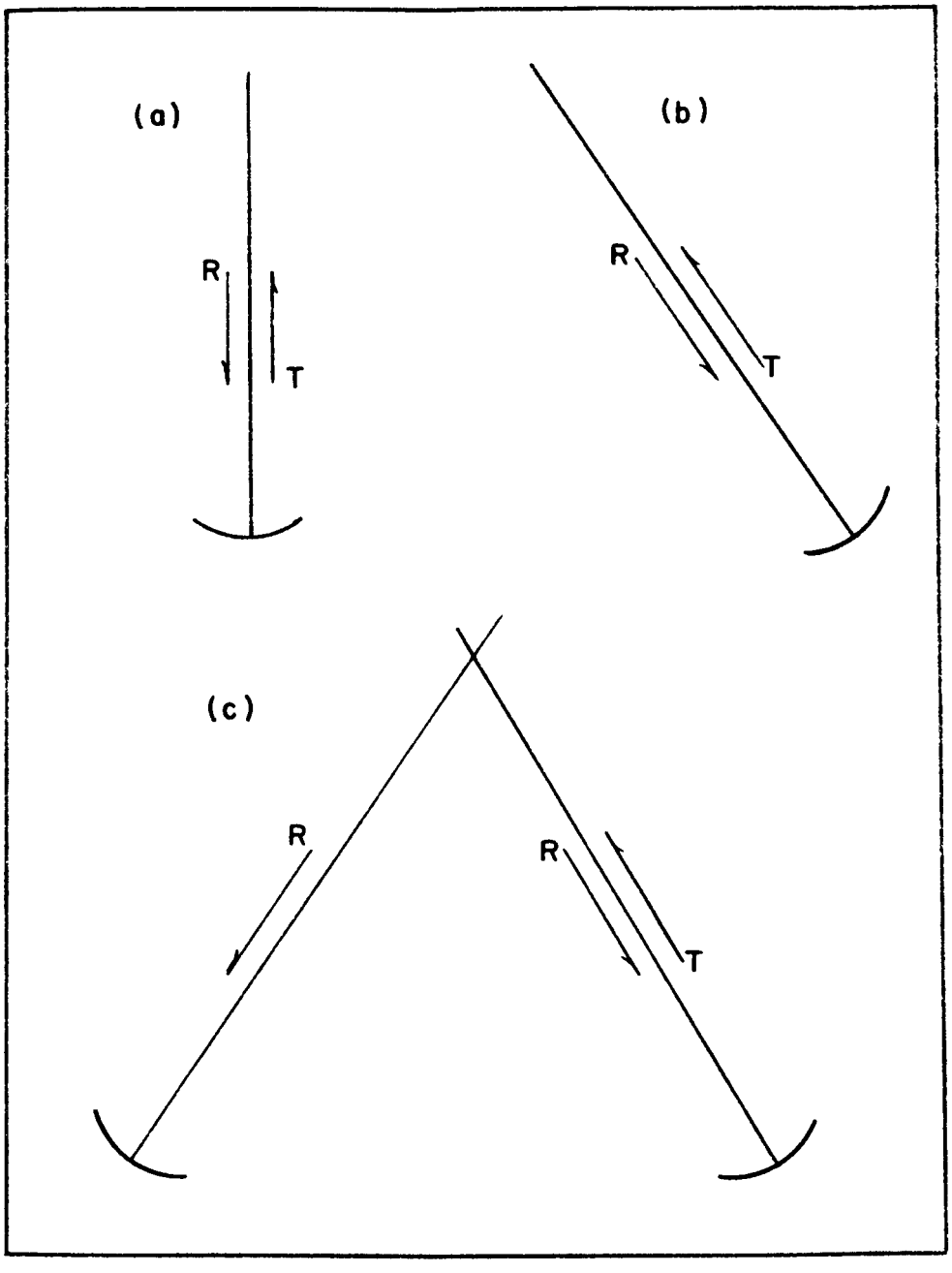

Fig. 1. Acoustic radar configurations. (a) Vertically directed monostatic. (b) Inclined monostatic. (c) Bistatic. T indicates transmitted acoustic energy. R indicates received acoustic energy.

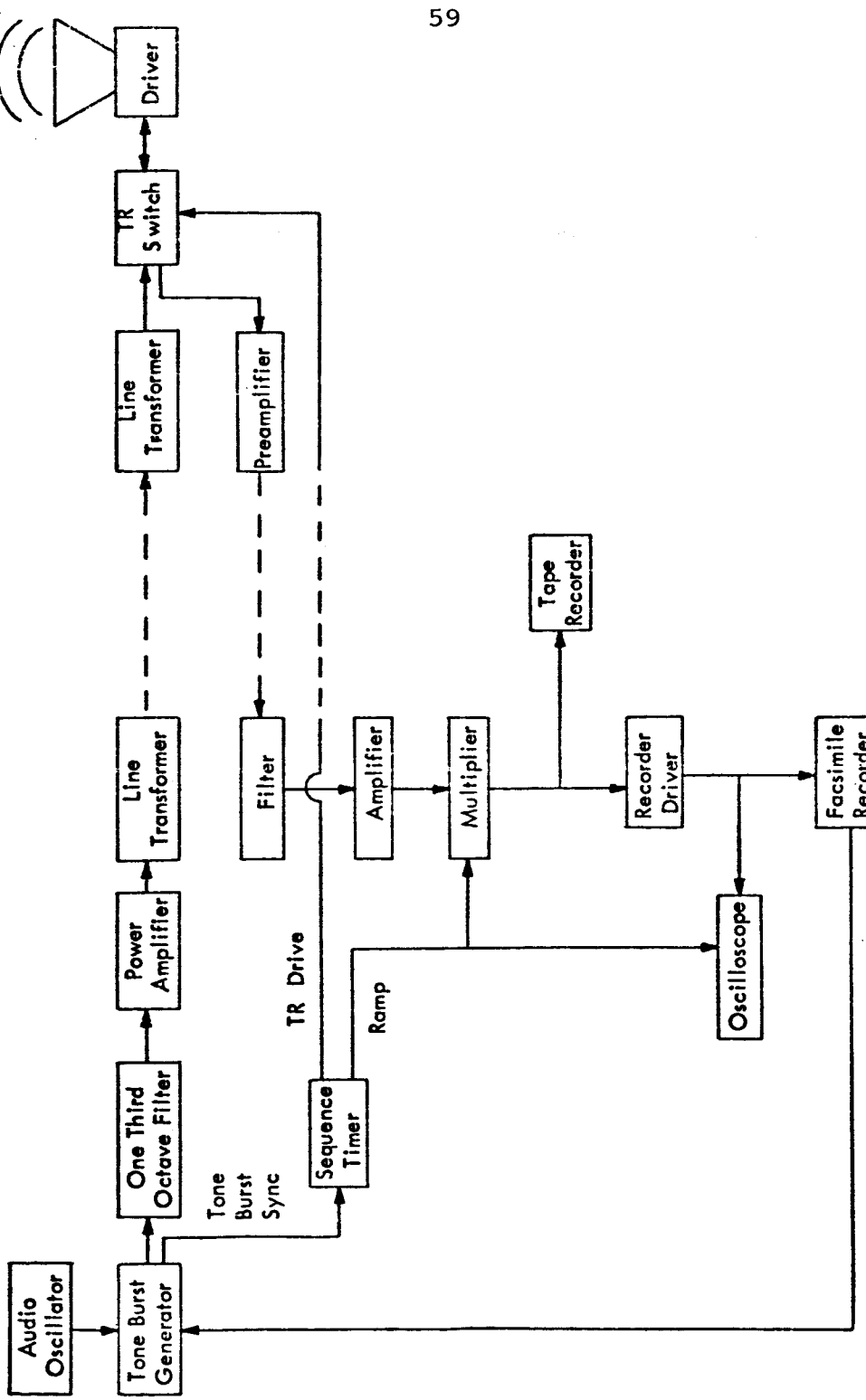

Fig. 2. Block Diagram of the Acoustic Radar (Cronenwett et al, 1972).

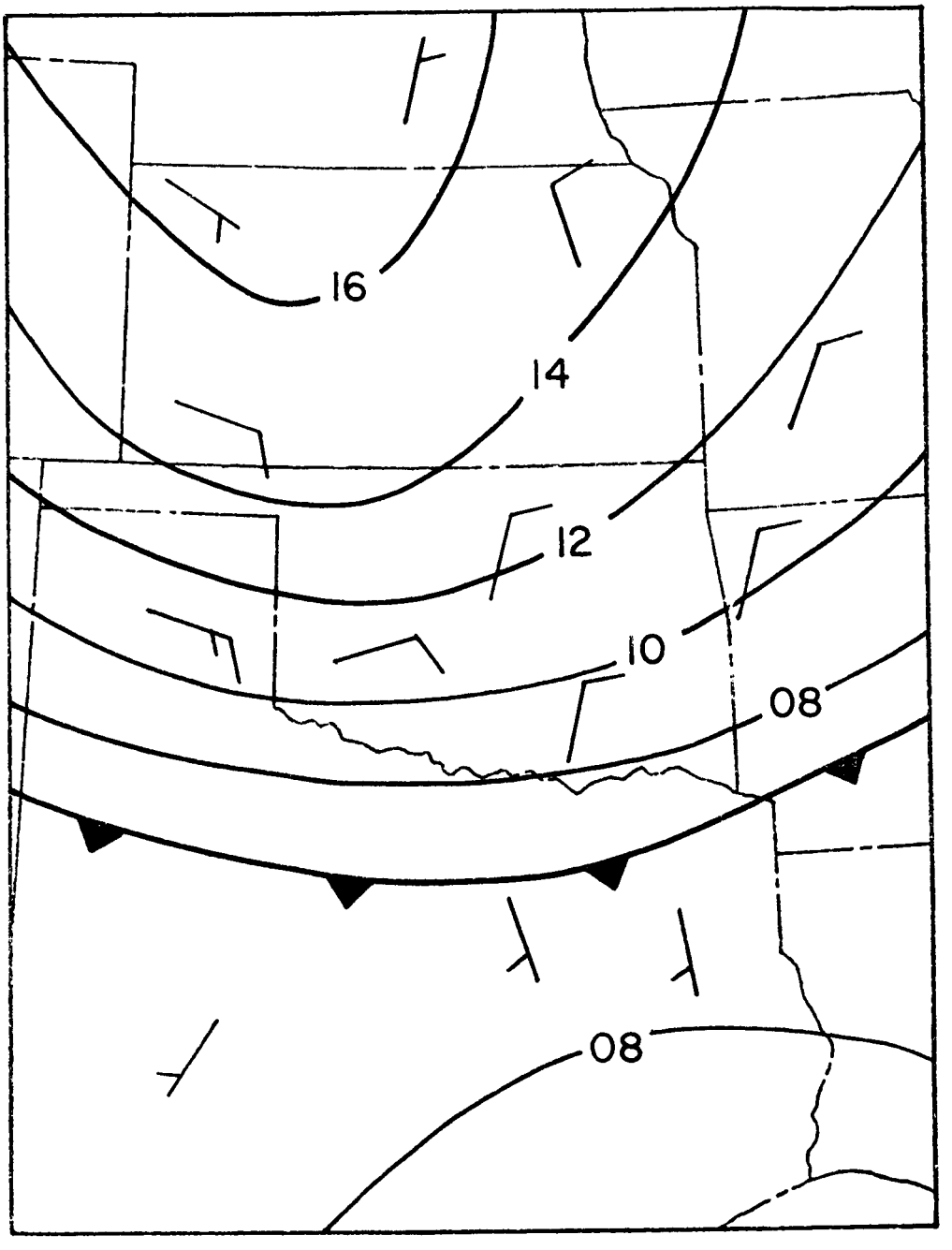

Fig. 3. Surface analysis for 0000 CST 21 June 1972 (isobars labeled in mb, i.e., 12 = 1012 mb).

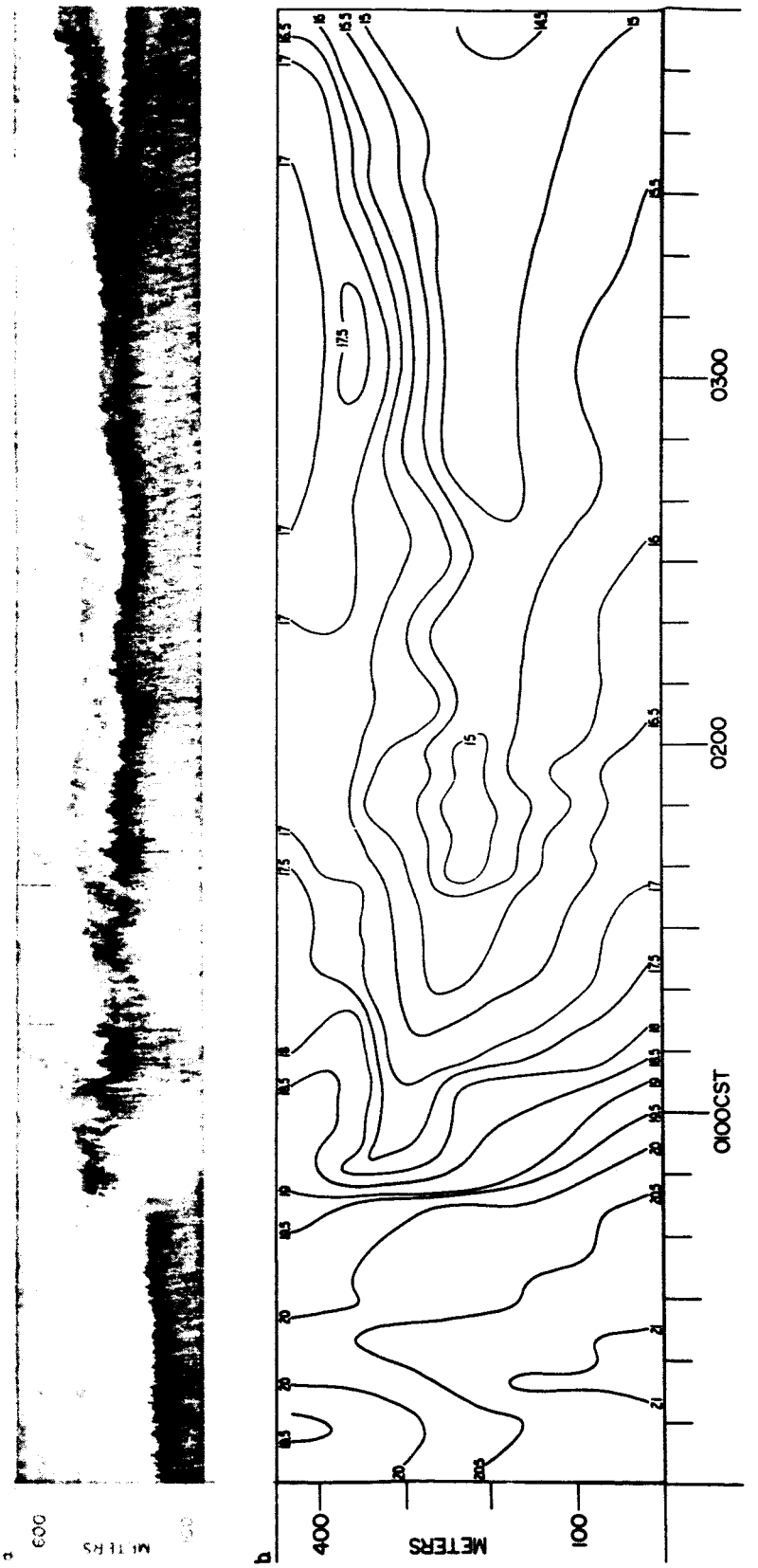

Fig. 4. Acoustic radar facsimile record (a) and time section of temperature (°C) (b) for 0000-0400 CST 21 June 1972.

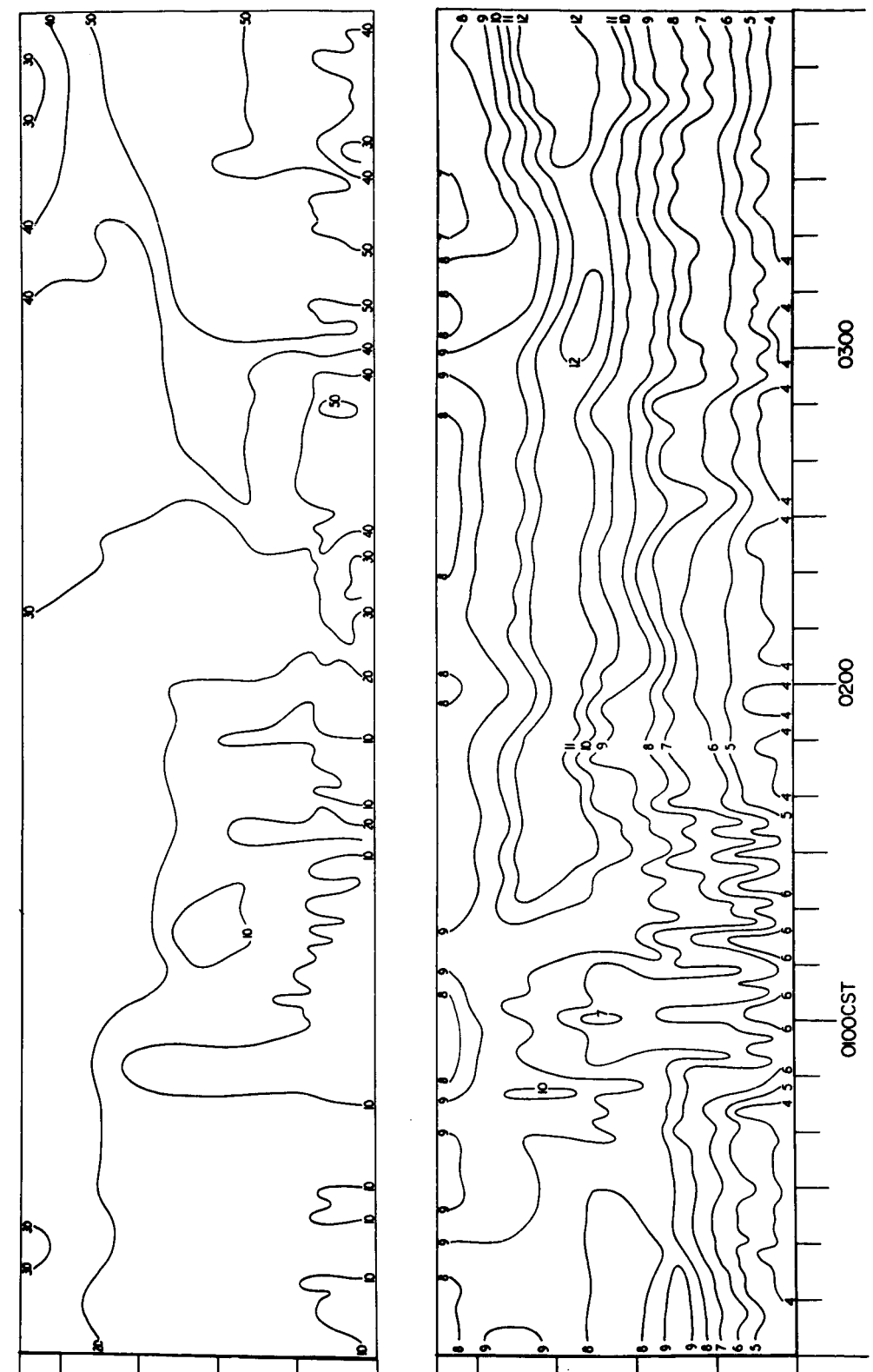

Fig. 4. Time section of wind direction (degrees) (c) and wind speed (m sec^{-1}) (d) for 0000-0400 CST 21 June 1972.

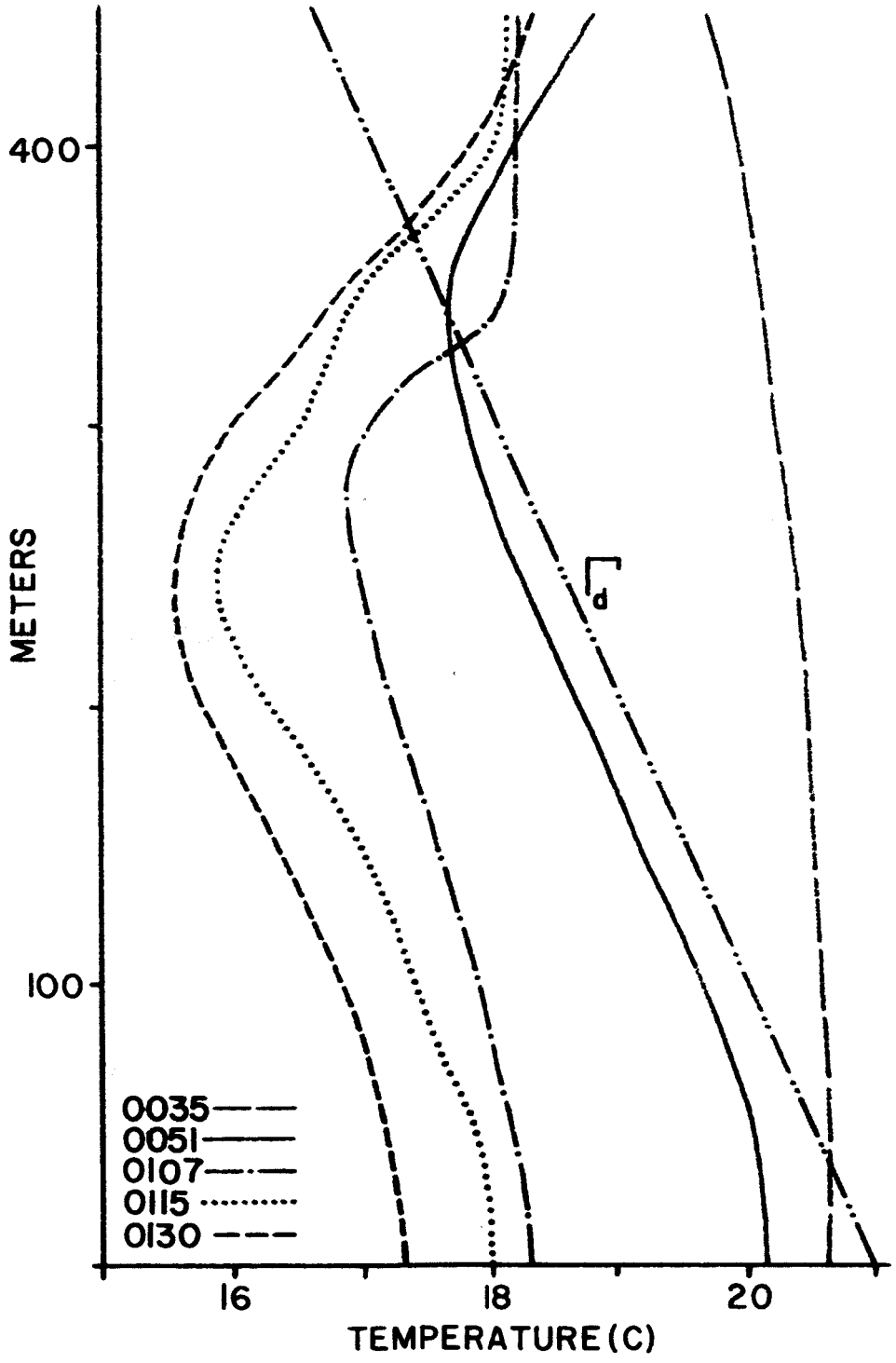

Fig. 5. Temperature profiles (°C) for 0035, 0051, 0107, 0115, and 0130 CST 21 June 1972. Γ_d profile is the dry adiabatic lapse rate.

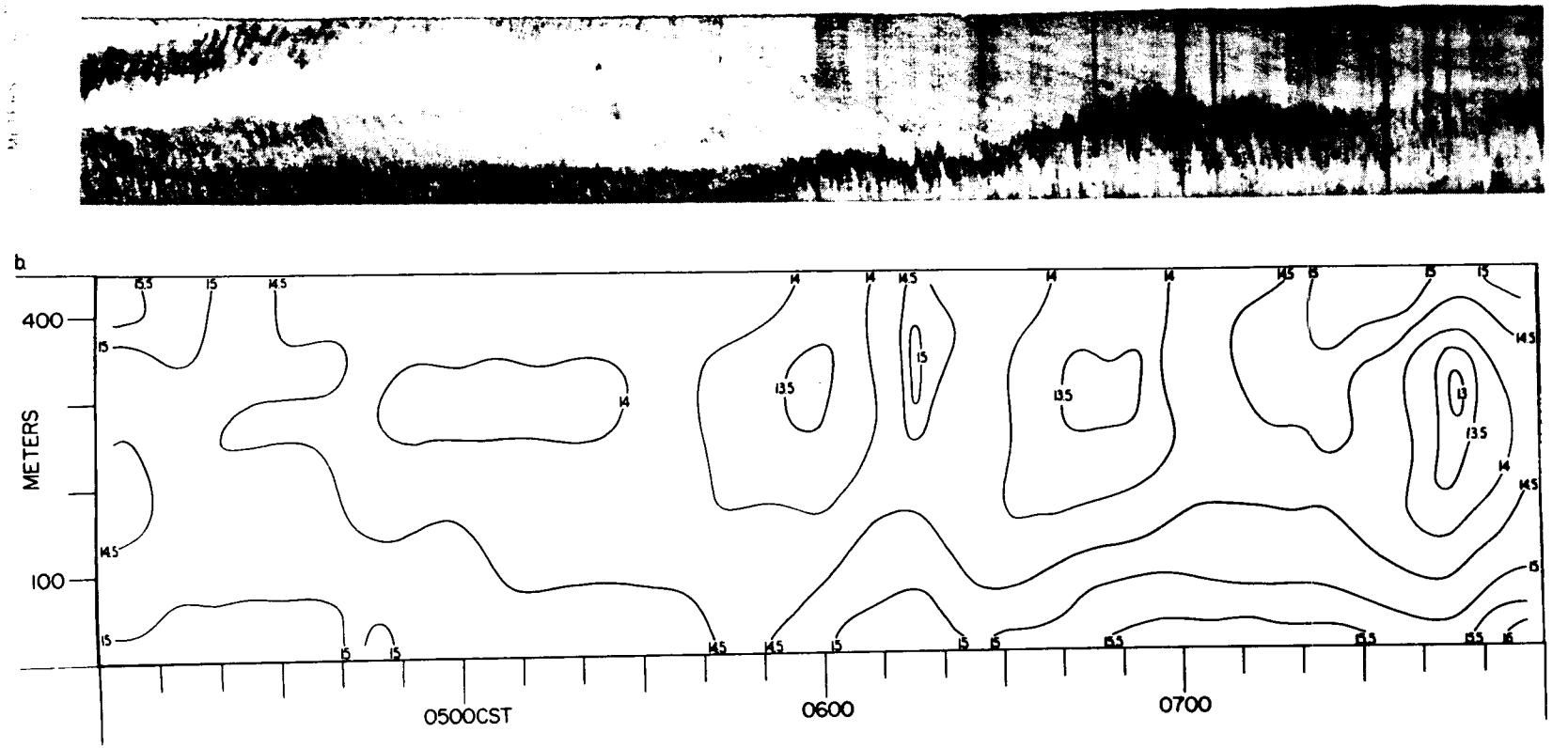

Fig. 6. Acoustic radar facsimile record (a) and time section of temperature (°C) (b) for 0400-0800 CST 21 June 1972.

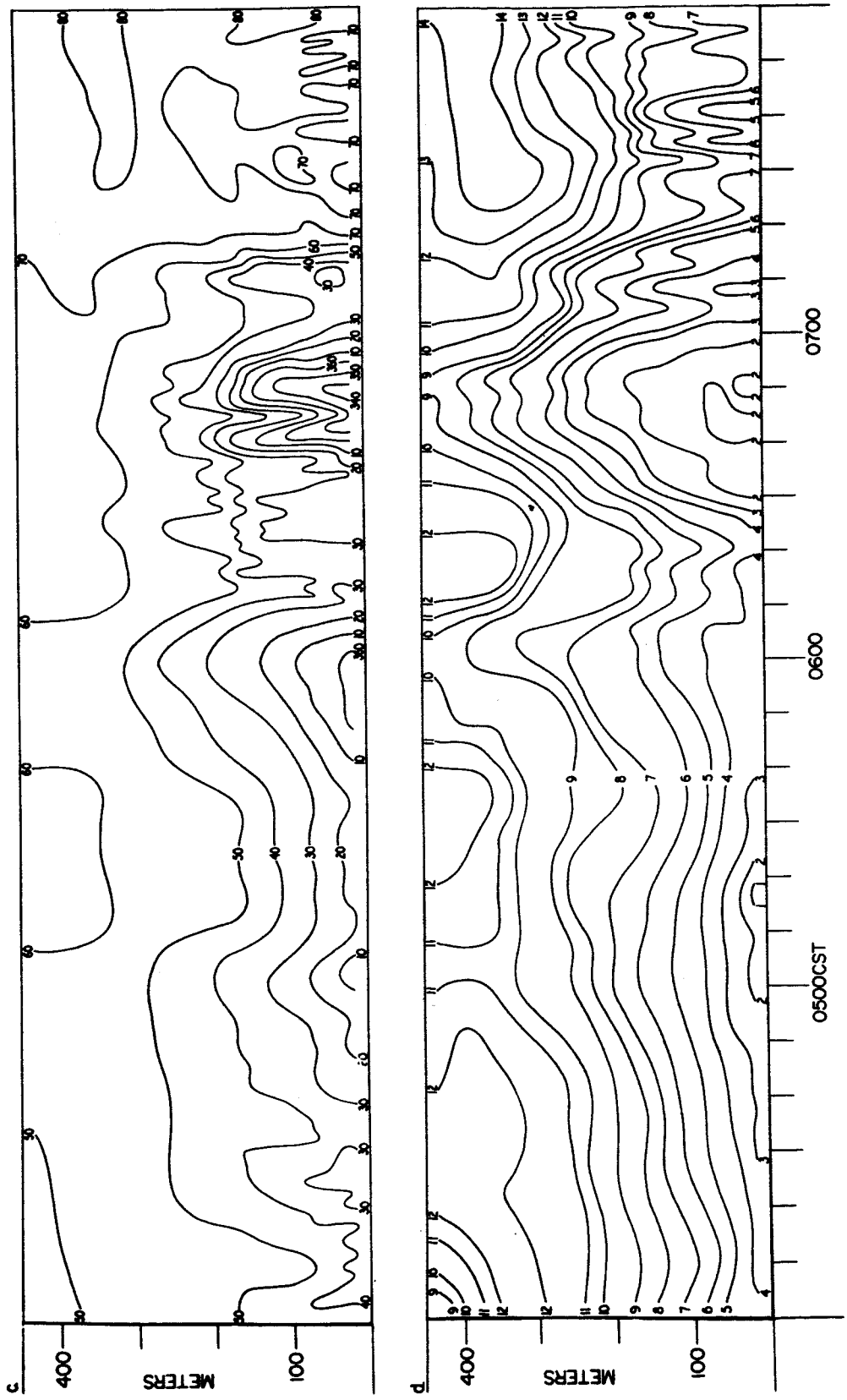

Fig. 6. Time section of wind direction (degrees) (c) and wind speed (m sec^{-1}) (d) for 0400-0800 CST 21 June 1972.

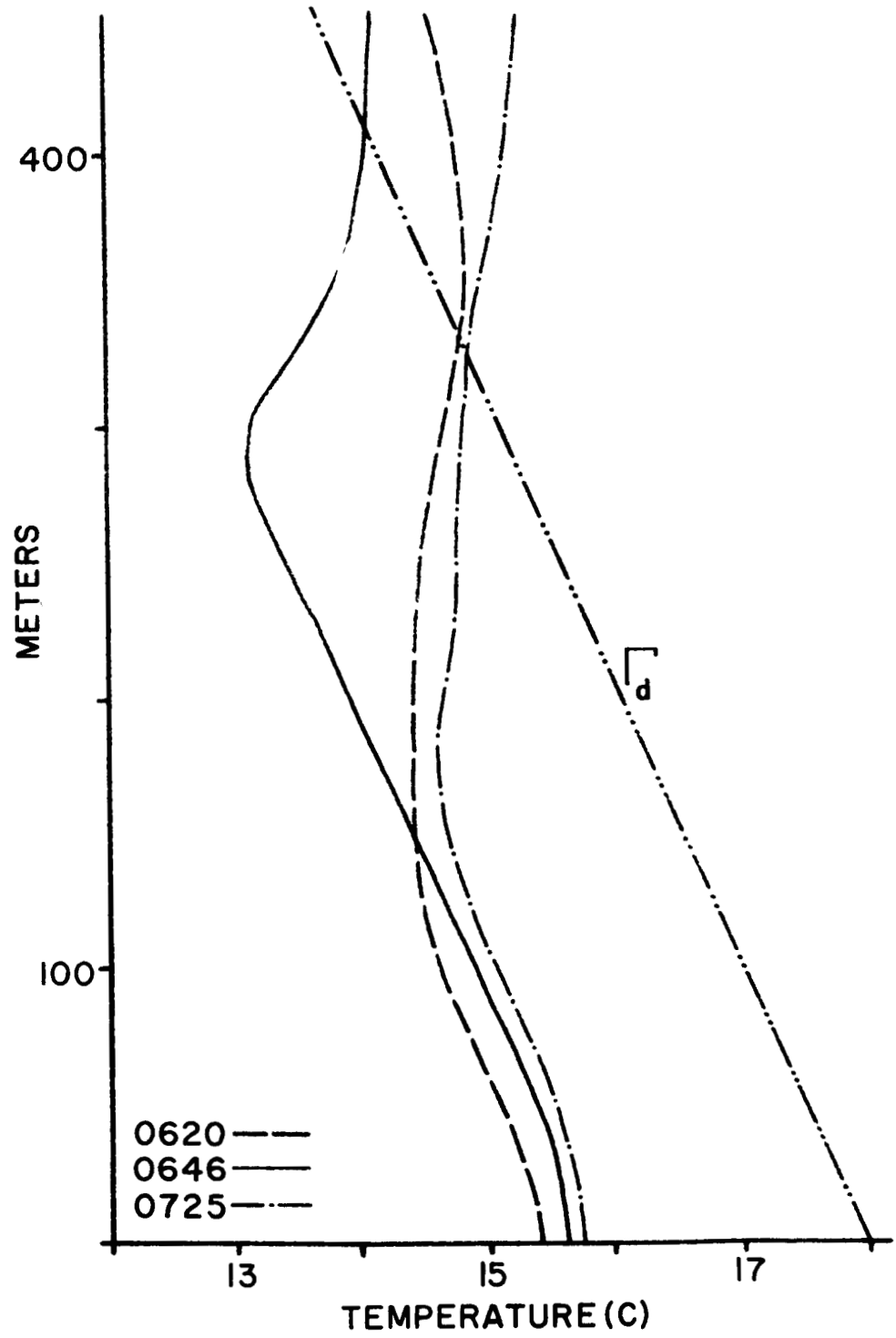

Fig. 7. Temperature profiles (°C) for 0620, 0646, and 0725 CST 21 June 1972. Γ_d profile is the dry adiabatic lapse rate.

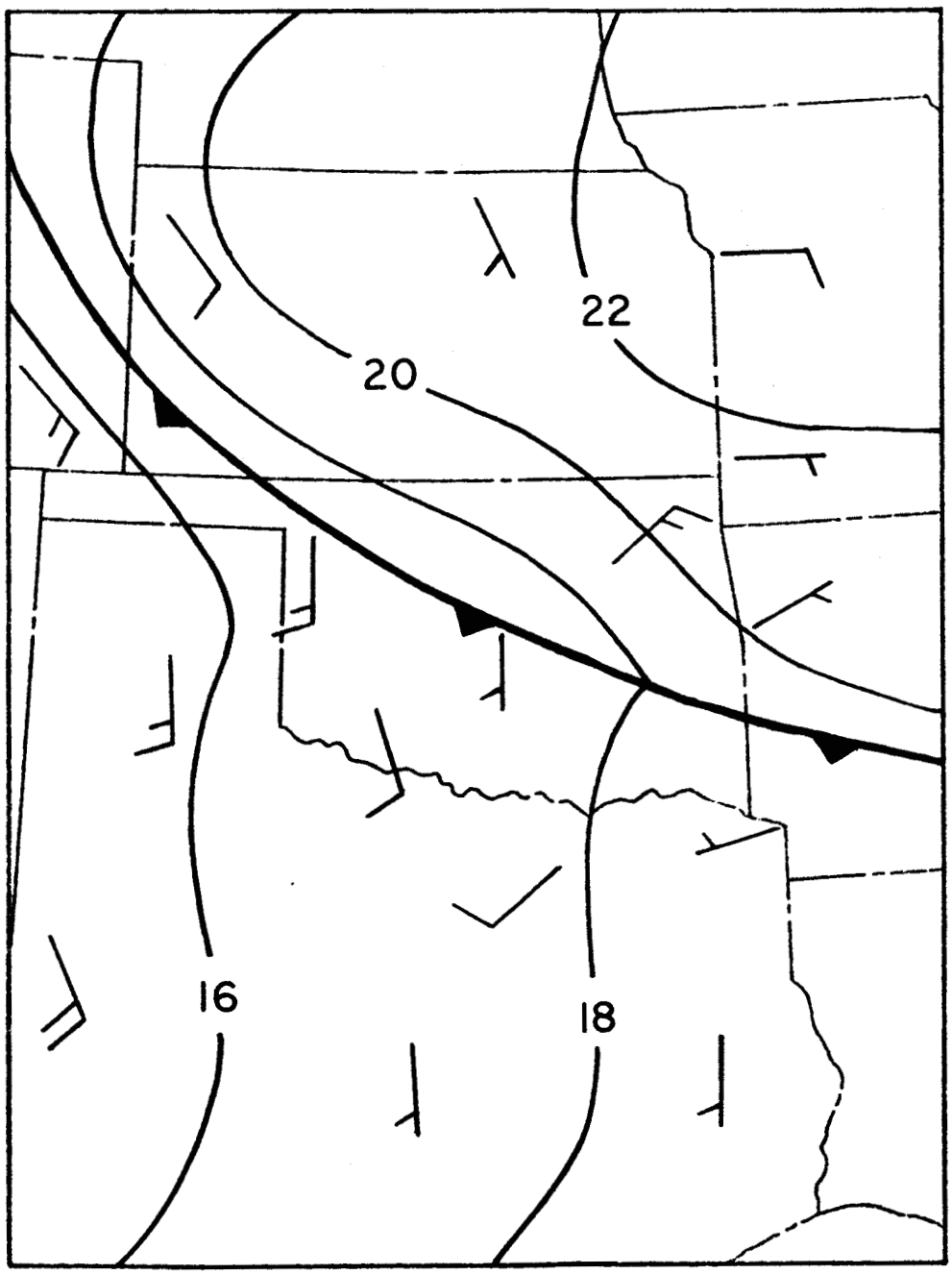

Fig. 8. Surface analysis for 1700 CST 4 August 1972 (isobars labeled in mb, i.e., 18 = 1018 mb).

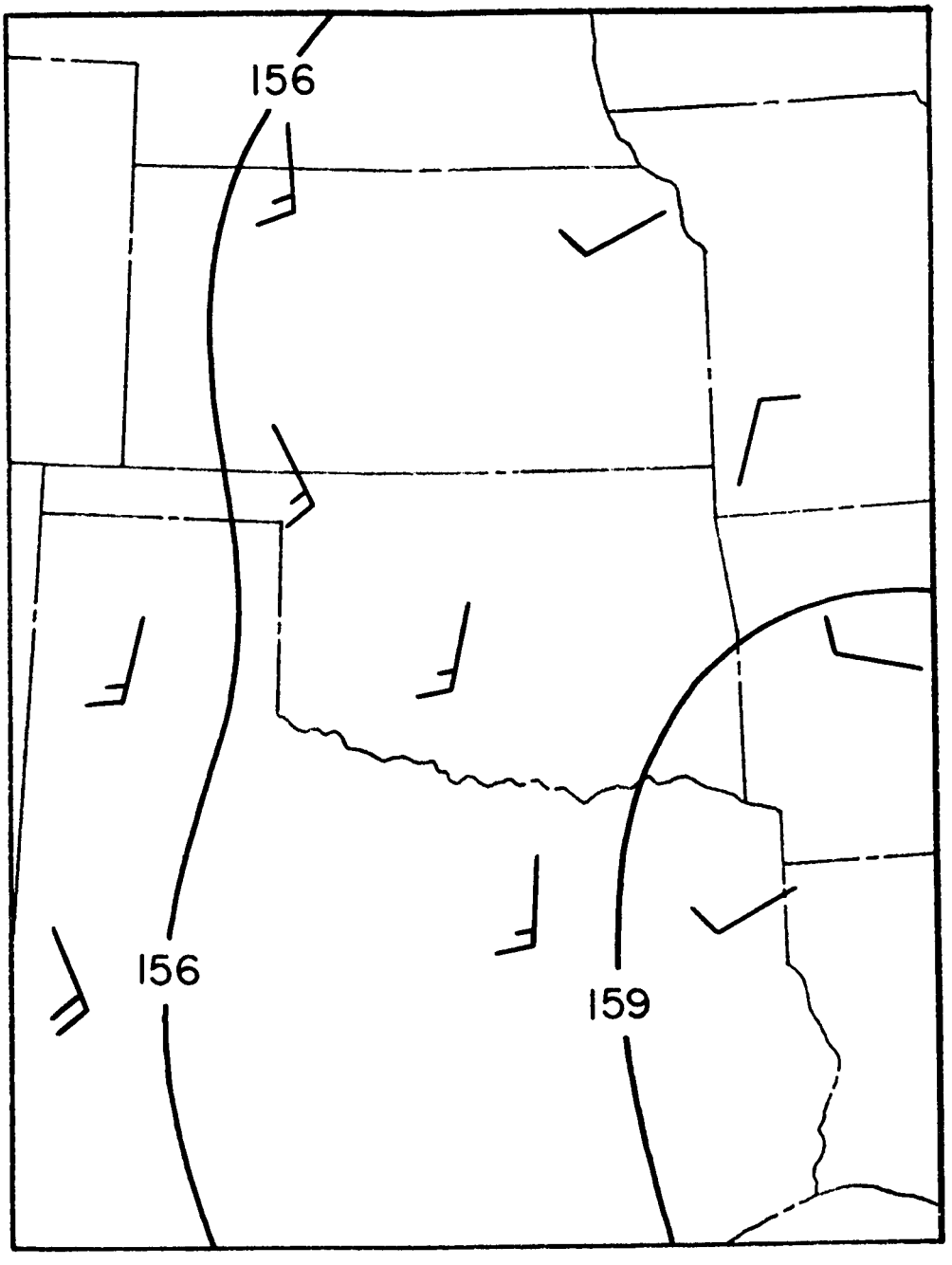

Fig. 9. Height contour pattern at the 850-mb level for 1800 CST 4 August 1972 (contour interval is 30 m).

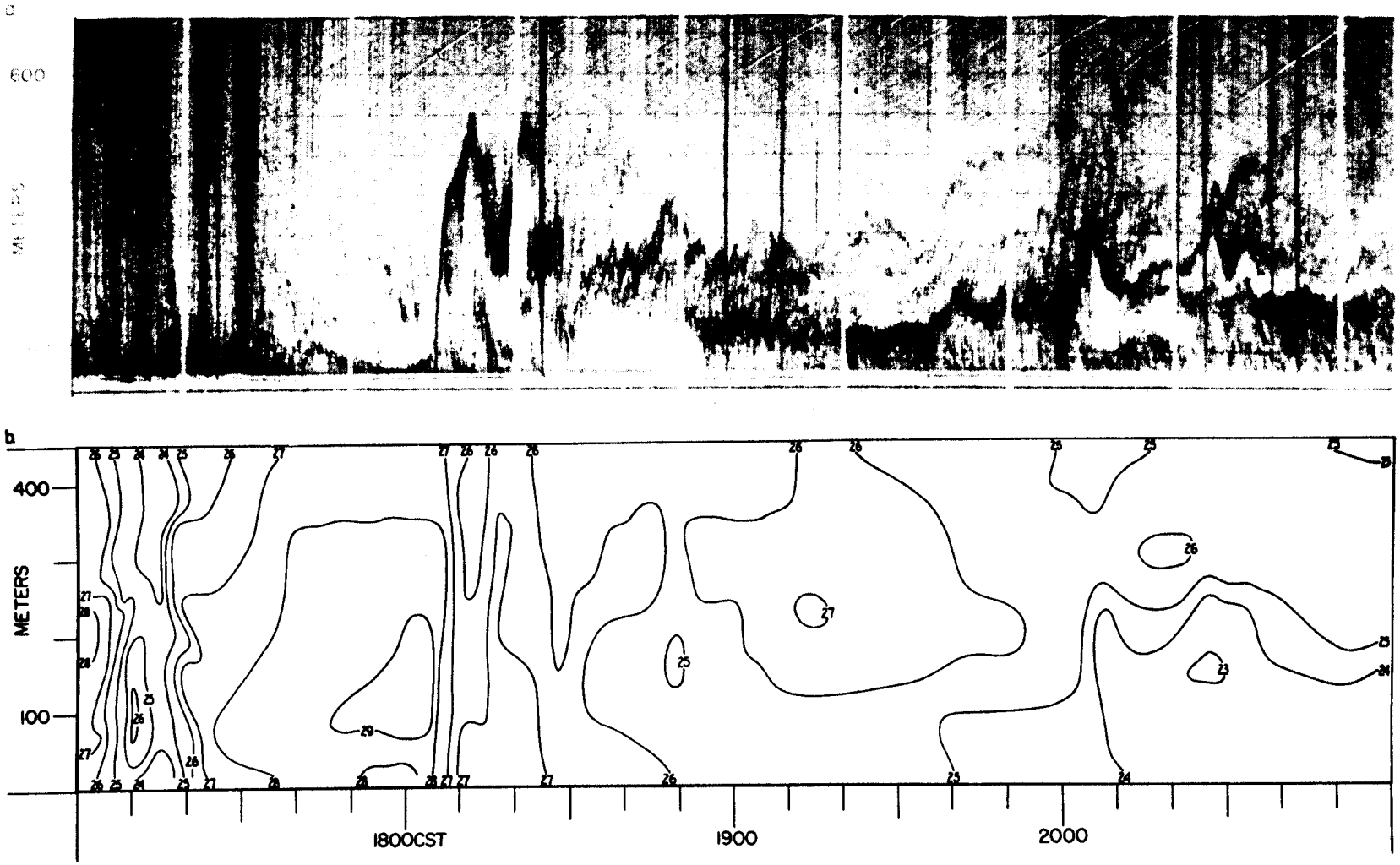

Fig. 10. Acoustic radar facsimile record (a) and time section of temperature (°C) (b) for 1700-2100 CST 4 August 1972.

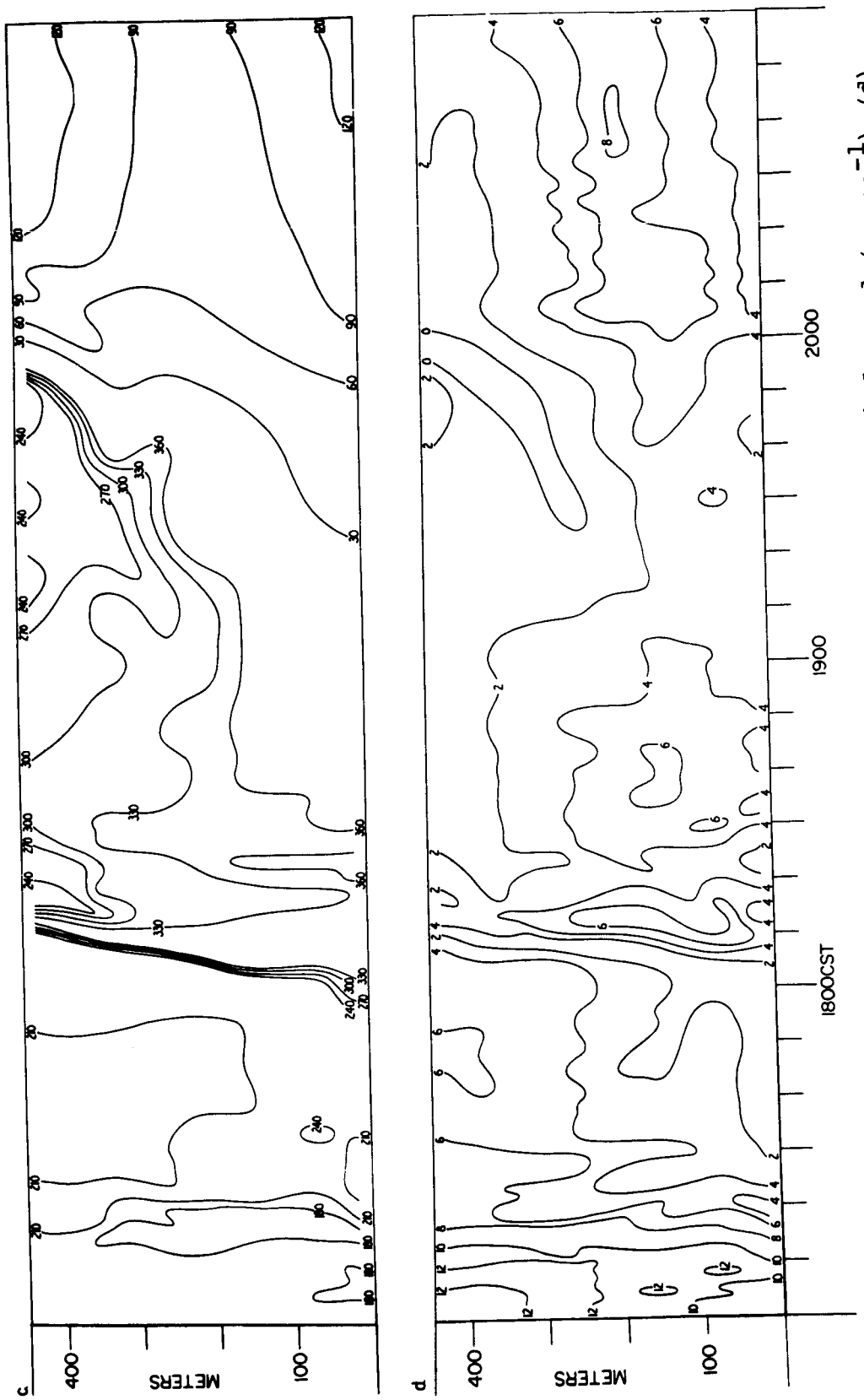

Fig. 10. Time section of wind direction (degrees) (c) and wind speed (m sec^{-1}) (d) for 1700-2100 CST 4 August 1972.

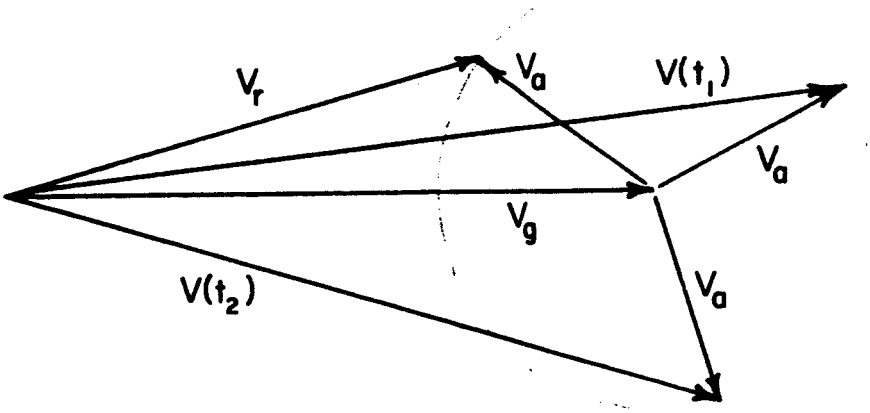

Fig. 11a. Schematic diagram of the inertial oscillation and its effect on the boundary layer winds. $V(t_1)$ and $V(t_2)$ are predicted real winds for times t_1 and t_2.

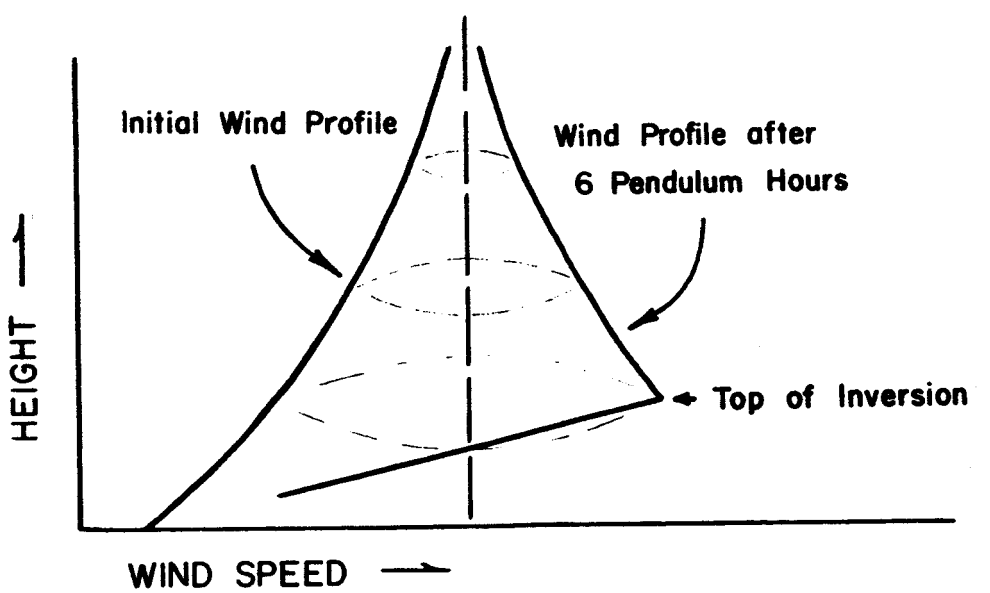

Fig. 11b. Schematic illustration explaining the evolution of a boundary layer jet profile (Blackadar, 1957).

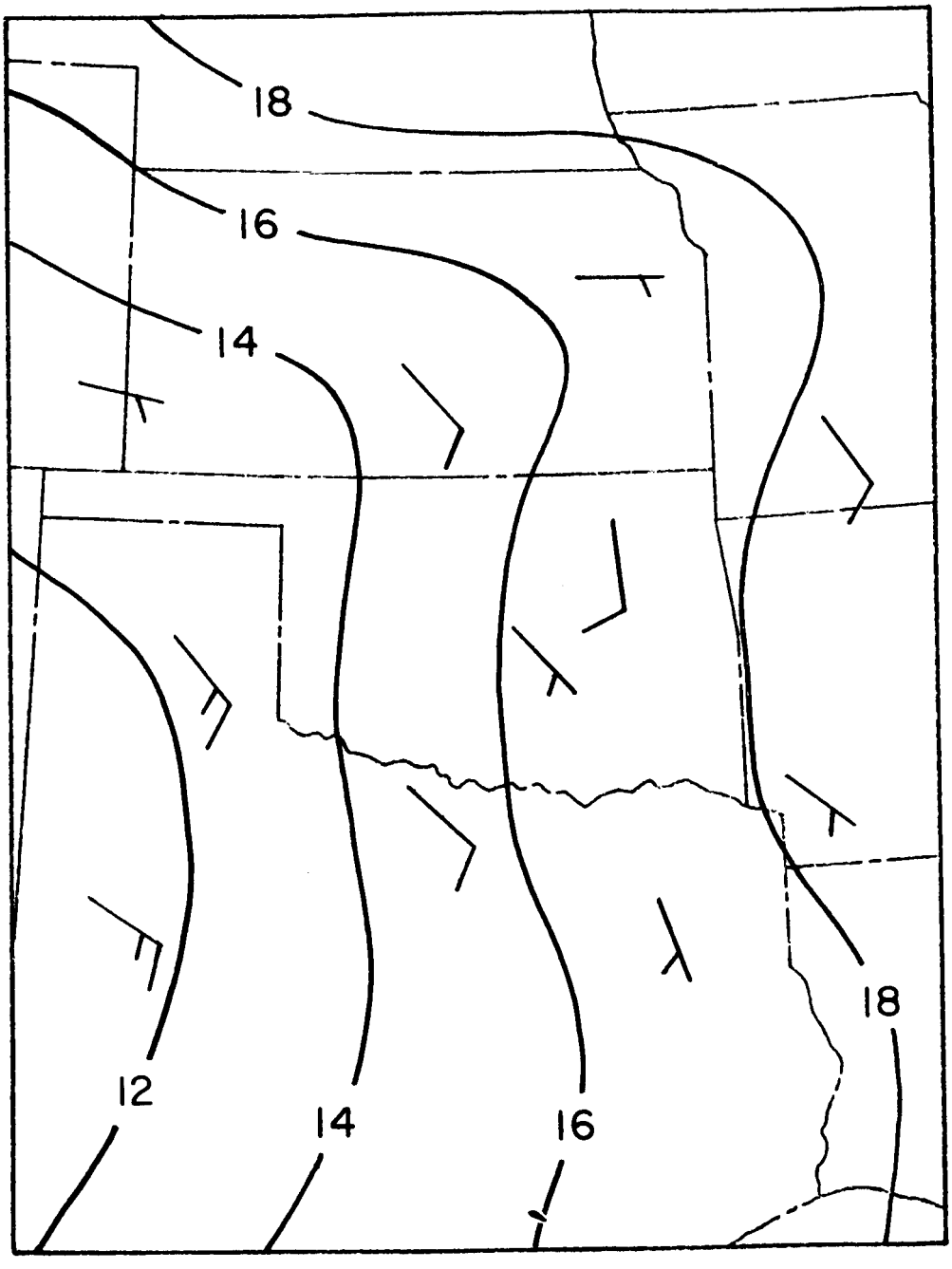

Fig. 12a. Surface analysis for 0000 CST 1 August 1972 (isobars labeled in mb, i.e., 16 = 1016 mb).

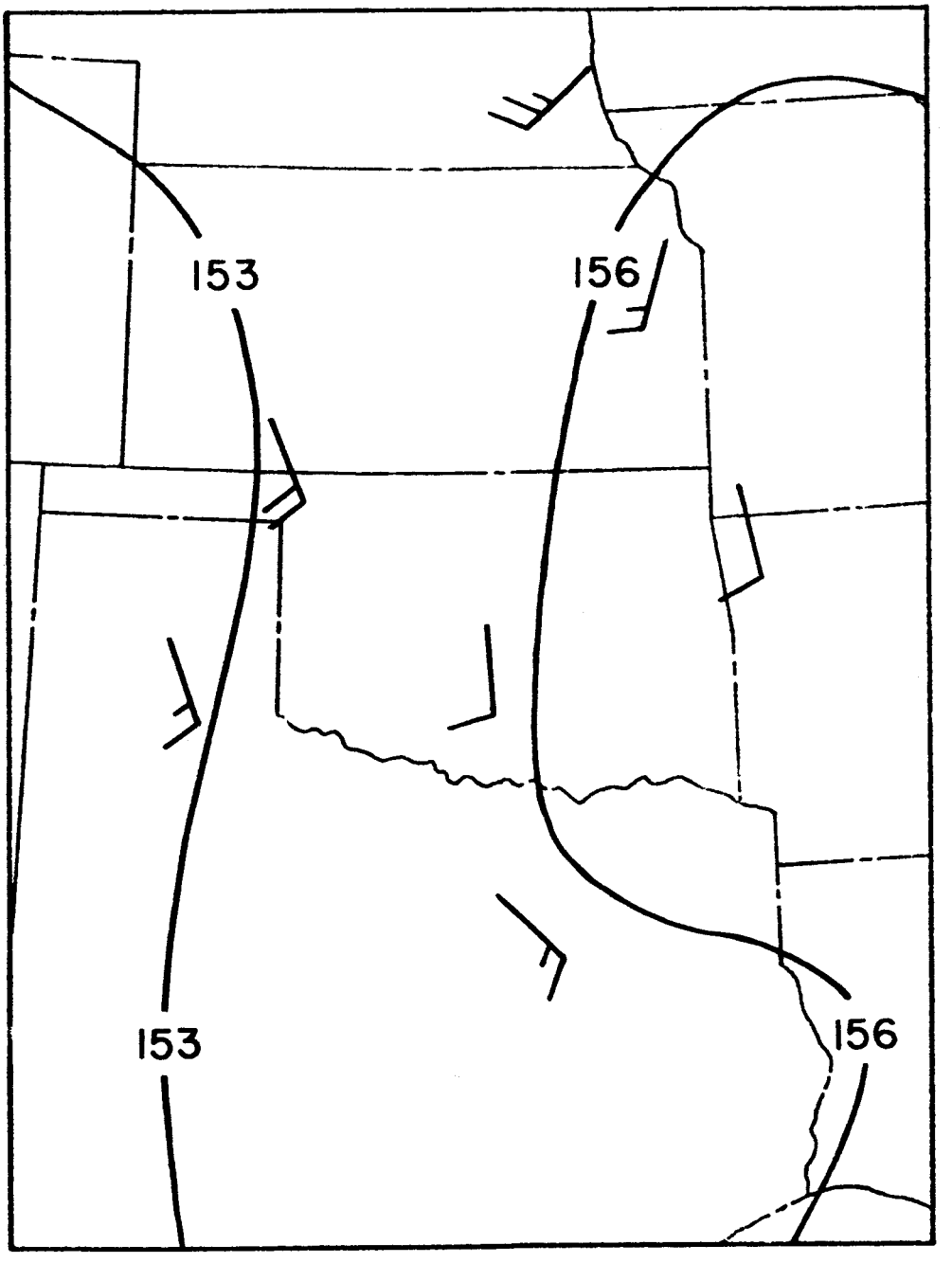

Fig. 12b. Height contour pattern at the 850-mb level for 1800 CST 31 July 1972 (contour interval is 30 m).

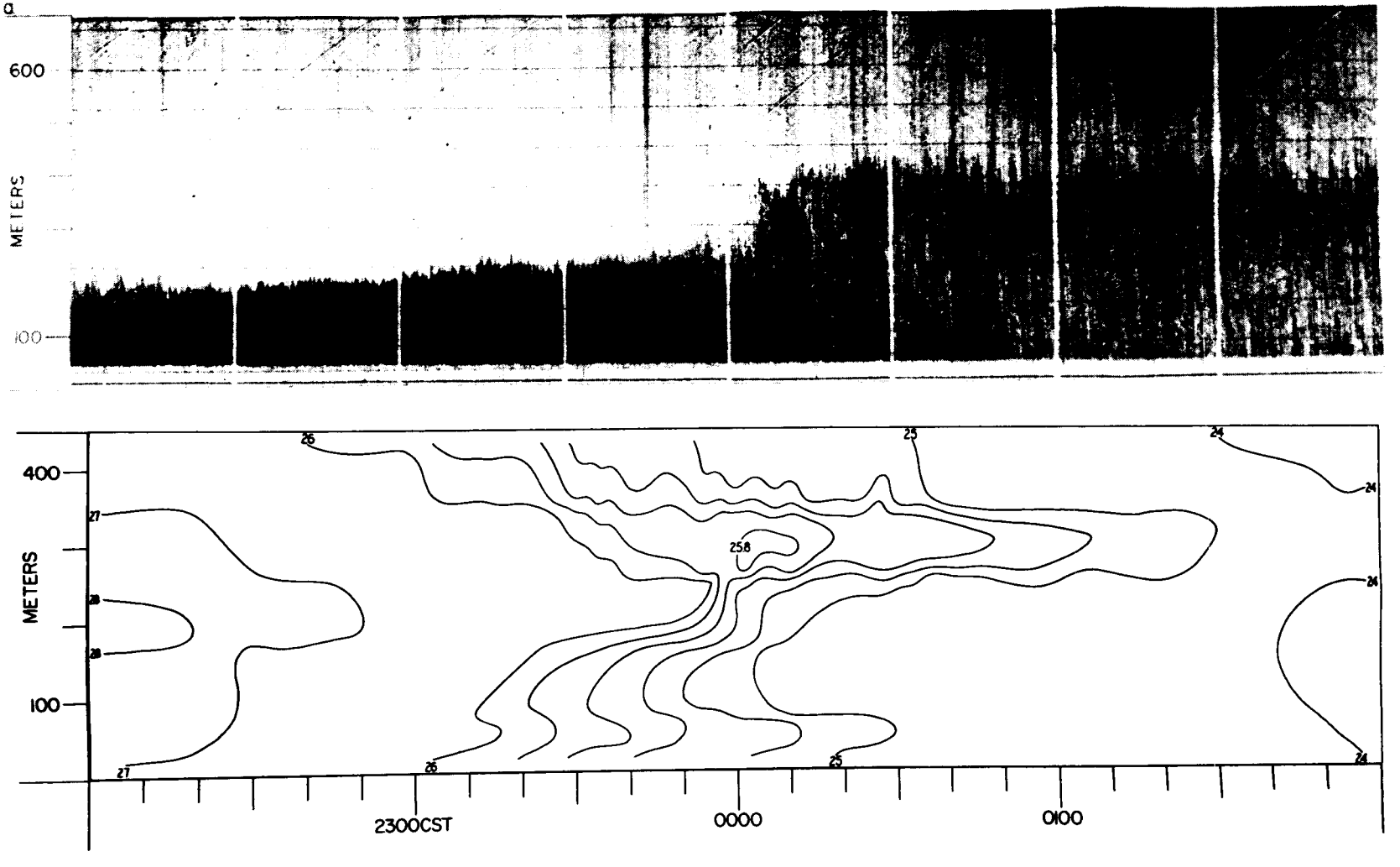

Fig. 13. Acoustic radar facsimile record (a) and time section of temperature (°C) (b) for 2200 CST 31 July-0200 CST 1 August 1972 (isotherms are at intervals of 0.2 °C between 25 and 26 °C).

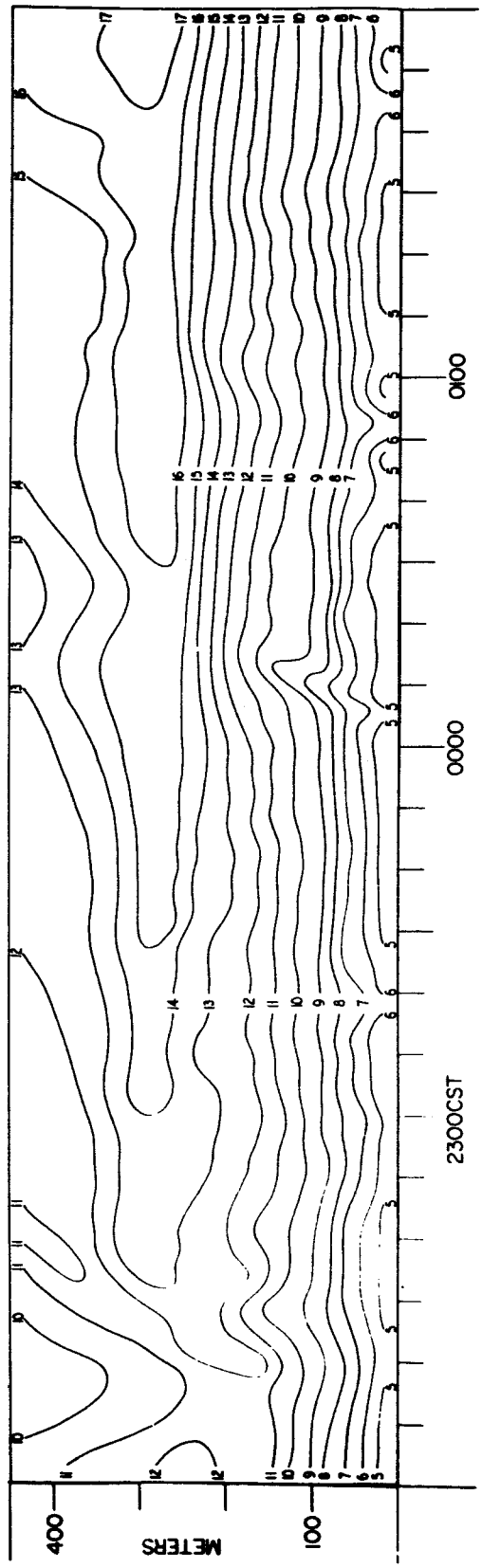

Fig. 13c. Time section of wind speed (m sec^{-1}) for 2200 CST 31 July-0200 CST 1 August 1972.

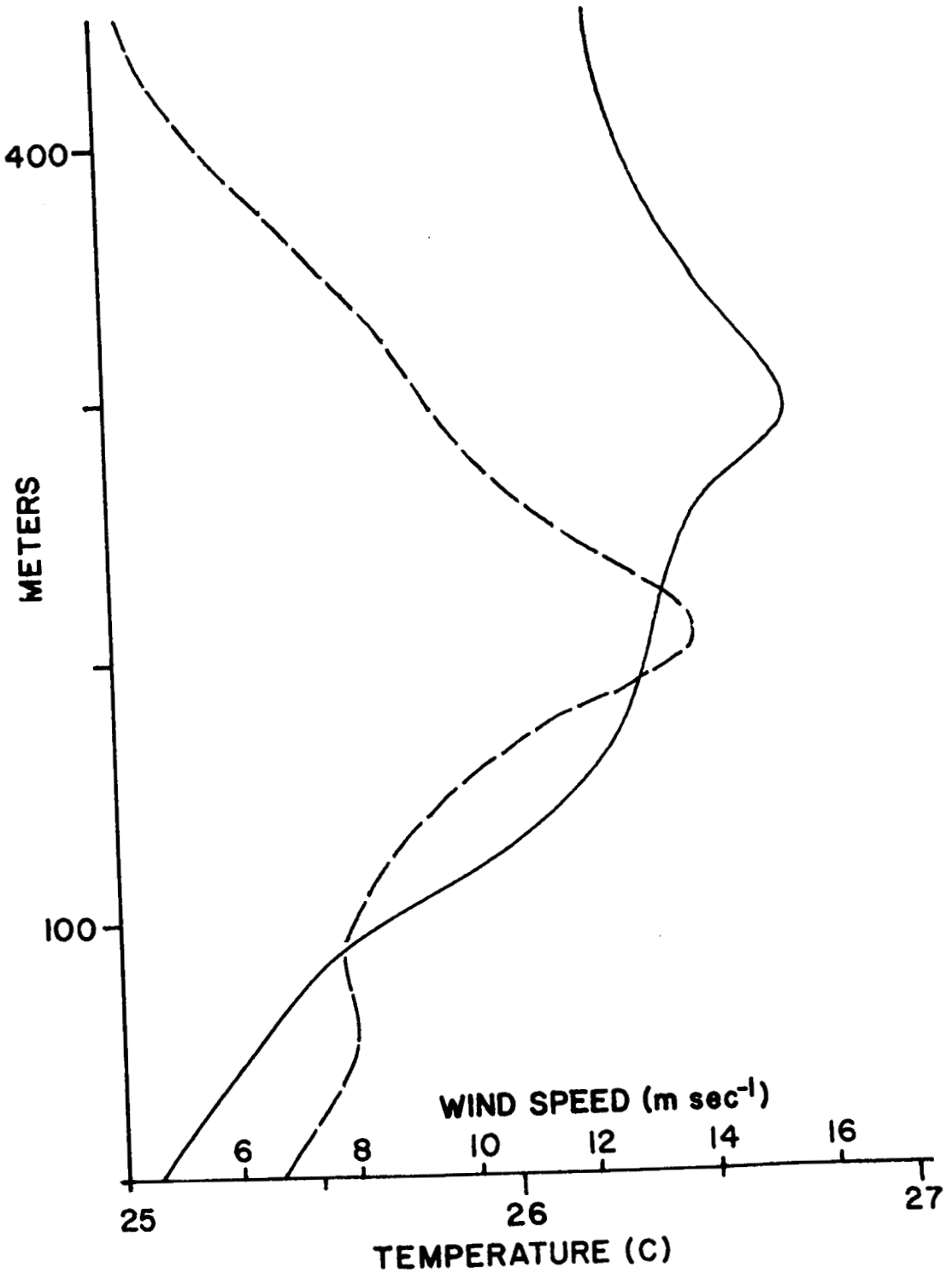

Fig. 14. Temperature (°C) and wind speed (m sec^{-1}) profiles for 2330 CST 31 July 1972.

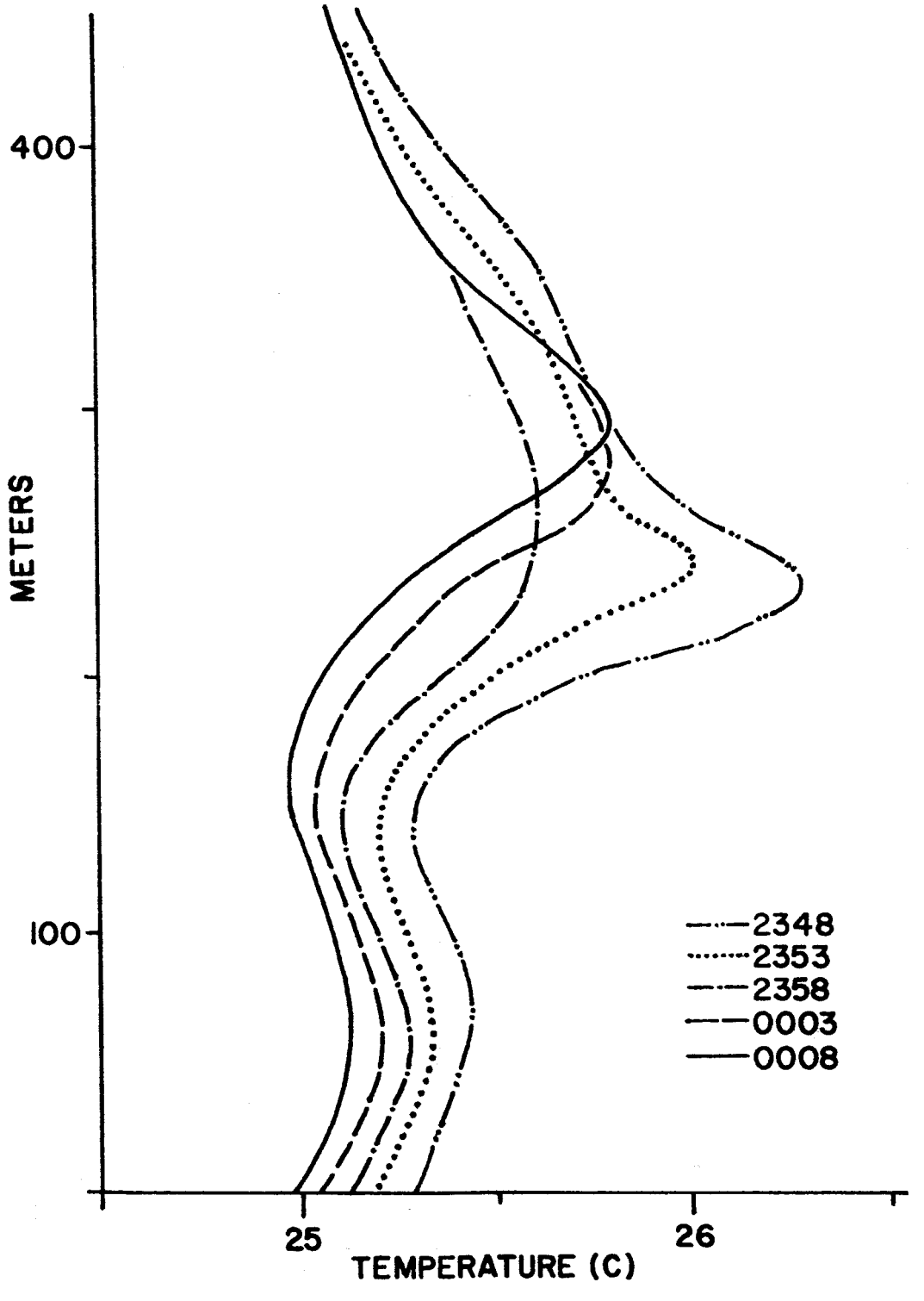

Fig. 15. Temperature profiles (°C) at 5-min intervals from 2348 CST 31 July to 0008 CST 1 August 1972.

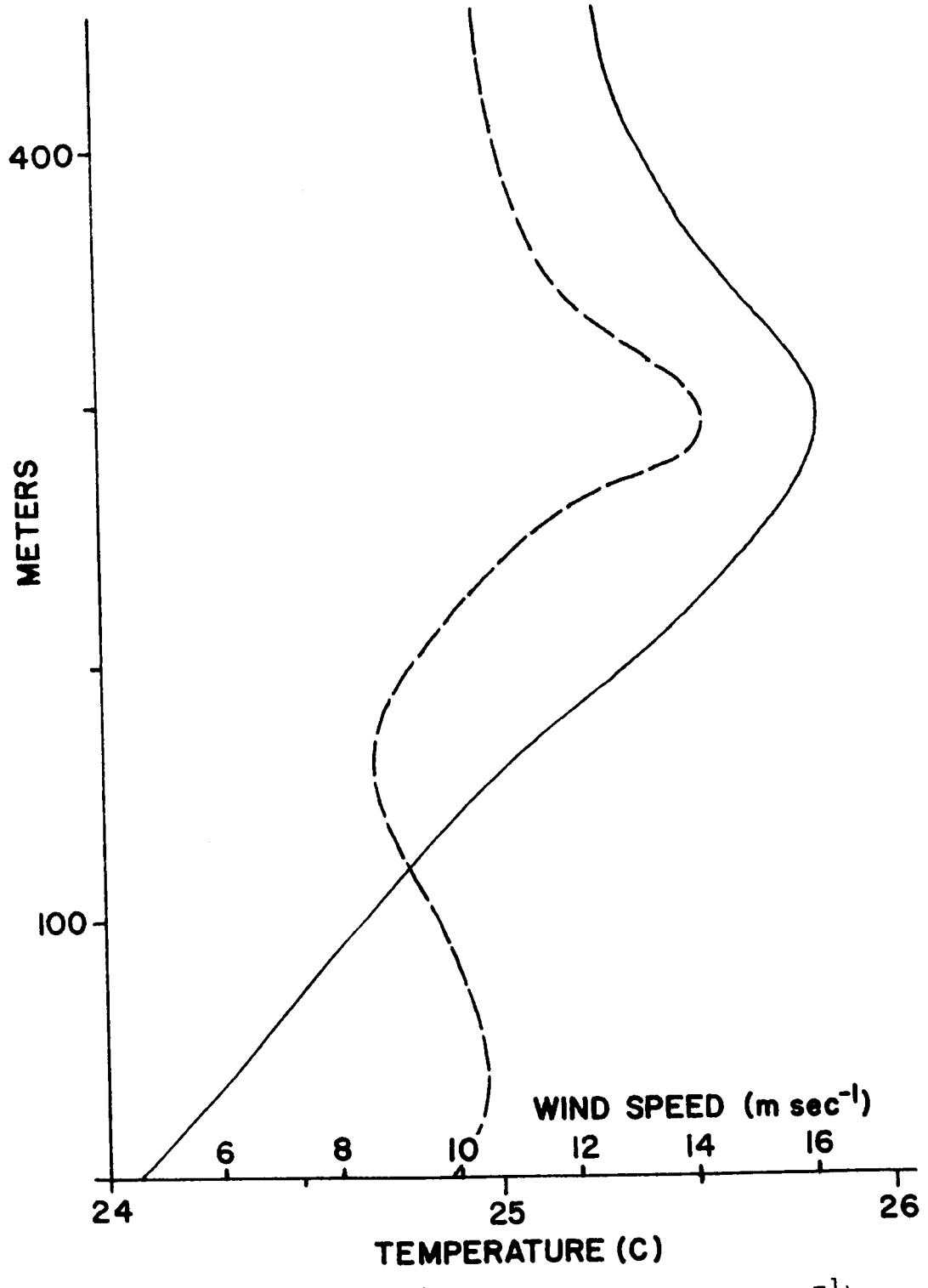

Fig. 16. Temperature (°C) and wind speed (m sec^{-1}) profiles for 0032 CST 1 August 1972.

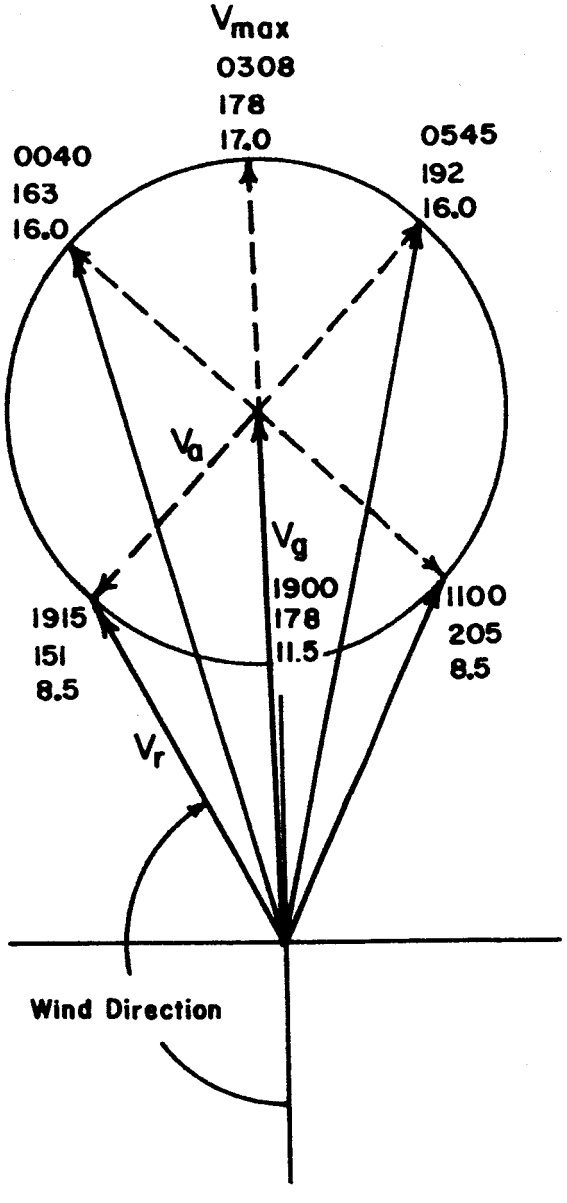

Fig. 17. Application of the inertial oscillation to the real (V_r) and geostrophic (V_g) winds as determined near sunset 31 July 1972. Given are the valid time (CST), wind direction (degrees), and wind speed (m sec^{-1}), i.e., at 0545 CST the wind was predicted to be from 192° at a speed of 16.0 m sec^{-1}.

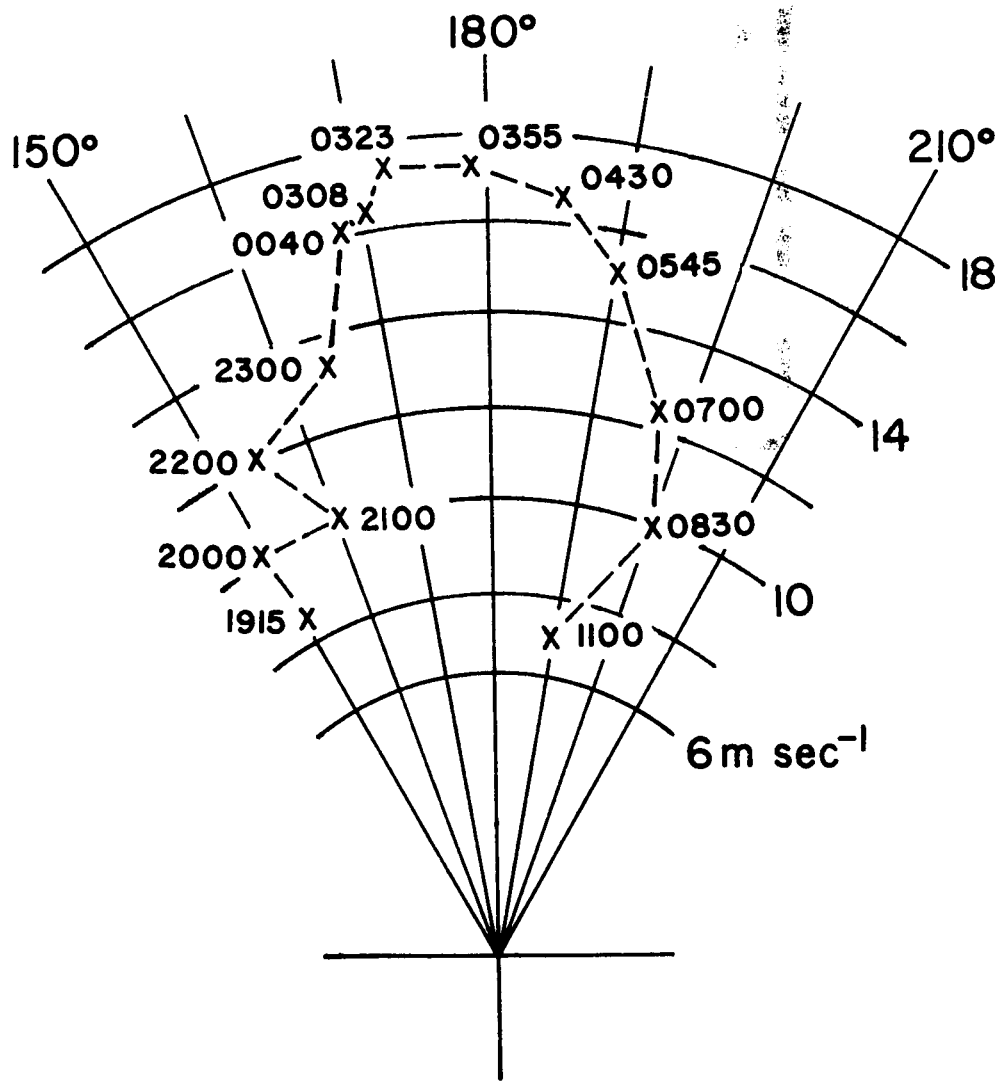

Fig. 18. Hodograph of observed winds for 31 July-1 August 1972. Isotachs are at intervals of 2 m sec^{-1}. Isolines of wind direction are at intervals of 10 degrees. Times are CST.

NASA-Langley, 1974